CROP MONITORING USING MULTISPECTRAL AND HYPERSPECTRAL REMOTE SENSING

MS(R) Thesis

By

Yash Raj



DEPARTMENT OF ASTRONOMY, ASTROPHYSICS AND SPACE ENGINEERING

INDIAN INSTITUTE OF TECHNOLOGY INDORE

May, 2026

CROP MONITORING USING MULTISPECTRAL AND HYPERSPECTRAL REMOTE SENSING

A THESIS

Submitted in partial fulfillment of the
requirements for the award of the degree
of

MS(R) Thesis

by

Yash Raj



DEPARTMENT OF ASTRONOMY,ASTROPHYSICS AND SPACE ENGINEERING
INDIAN INSTITUTE OF TECHNOLOGY INDORE

CANDIDATE'S DECLARATION

I hereby certify that the work which is being presented in the thesis entitled **CROP MONITORING USING MULTISPECTRAL AND HYPERSPECTRAL REMOTE SENSING** in partial fulfillment of the requirements for the award of the degree of MS(R) and submitted in the DEPARTMENT OF ASTRONOMY, ASTROPHYSICS AND SPACE ENGINEERING, Indian Institute of Technology Indore, is an authentic record of my work carried out during the period from **August 2024** to **July 2026** under the supervision of **Dr. Unmesh Khati, Assistant Professor, IIT Indore**

The matter presented in this thesis has not been submitted for the award of any other degree of this or any other institute.

Yash Raj (09/09/2026)
Signature
(Yash Raj)

This is to certify that the above statement made by the candidate is correct to the best of my knowledge.

Unmesh 09/09/2026
Signature of the Supervisor of MS Thesis
(Dr. Unmesh Khati)

Yash Raj has successfully given his MS(R) Oral Examination held on ...07/09/2026...

Unmesh
Signature of Thesis Supervisor
Date:- 09/09/2026

Manoneeta Chakraborty
Signature of Convener, DPGC
Date:- 9/9/2026

ACKNOWLEDGEMENTS

First of all, I thank my advisor, Dr. Unmesh khati, for his constant help and support throughout the work. I have learned a lot from him during the very fruitful discussions that have given me a lot of independence to pursue my ideas, and his suggestions at various stages of this work were immensely helpful, for which I am grateful to him. I am also thankful to the Department of Astronomy, Astrophysics, and Space Engineering, IIT Indore, for providing the atmosphere and essential resources for carrying out this project.

Abstract

Nutrient stress is a significant threat to crop yield quality and can cause soil infertility. In satellite-based remote sensing, accurately monitoring nutrient stress with optical sensors is often challenging due to spatial and temporal resolution constraints and atmospheric effects. To overcome the limitation of satellite data, UAV (Unmanned Aerial Vehicle)-based imaging is preferred. Hyperspectral imaging is a preferred approach for monitoring nutrient stress due to its sensitivity to plant chemical composition and its high spatial and temporal resolution. In this study, we performed an experiment involving nitrogen stress at underdose (60 kg/ha), recommended dose (120 kg/ha), and overdose (180 kg/ha) on wheat plants in a precision farm setup. The reflectance obtained from hyperspectral data allows for distinguishing between underdose (0.08–0.11 in 400 nm–700 nm, 0.3–0.38 in the NIR spectrum range), overdose (0.04–0.05 in 400 nm–700 nm, 0.42–0.55 in the NIR spectrum range), and recommended-dose (control) wheat plants. A comparative analysis was performed on data obtained with a UAV-based hyperspectral sensor and a handheld spectroradiometer for overdosed and underdosed nitrogen treatments. The results indicate a high correlation between the spectra obtained from both sensors, with r = 0.9841 for the underdose treatment and r = 0.9913 for the overdose treatment. Thus, a spectroradiometer can fill data gaps when hyperspectral data are unavailable. Additionally, we analysed pure vegetation pixels after masking out soil pixels for nutrient-sensitive indices (NDVI, NDRE, ND_{705}, $CL_{red-edge}$, and DATT). Our results indicate that ND_{705} and NDVI are optimal indicators for early nitrogen stress detection due to their high separability. The results were validated using an ANOVA test, in which ND_{705} had the lowest p-value (p = 0.007) for data acquired on 28 February 2025.

The second study investigates the use of UAV-mounted hyperspectral imaging for early-stage detection of Soybean Mosaic Virus (SMV) under field conditions near IIT Indore, India. Early detection of crop diseases is critical for minimizing yield losses and enabling timely intervention, particularly in soybean where viral infections can spread rapidly and remain unnoticed during initial stages. Hyperspectral data (400–1000 nm, 281 bands) were collected at three temporal stages: healthy (2nd August), slightly affected (6th August), and early symptomatic (12th August). The results show clear spectral separation across these stages. Compared to healthy conditions, reflectance increased by approximately 15–25% in the visible region and

up to 30% in the near-infrared (NIR) region during the early disease stage. spectral differences were detectable 4–6 days prior to visible symptom emergence, demonstrating the capability of hyperspectral data for early disease detection. These observations were validated through field inspection and RGB imagery. Overall, the study highlights that UAV-based hyperspectral sensing can reliably capture subtle physiological and structural changes in soybean canopies at an early stage. This provides a non-destructive and scalable approach for timely disease detection, supporting precision agriculture and improved crop management strategies.

Index Terms — abiotic stress, unmanned aerial vehicle(UAV), hyperspectral imaging(HSI), nitrogen stress, time series, vegetation index, soybean, early disease detection

Contents

ACKNOWLEDGEMENTS **2**

Abstract **3**

List of Figures **7**

1 Introduction **10**

1.1 Motivation 13

2 Review of Past Work and Problem Formulation **14**

2.1 Literature Review 14

2.2 Problem formulation for early stage nitrogen stress detection in wheat 16

2.3 Problem formulation for early soybean disease detection 16

3 Study Area **17**

3.1 Study area of wheat 17

3.2 Study area of soybean 18

4 MATERIAL AND METHOD **20**

4.1 Field data 20

4.2 UAV data 22

4.3 A detailed workflow 25

5 RESULTS AND DISCUSSION **26**

5.1 Preprocessing of hyperspectral data 26

5.2 Variation in wheat canopy spectral reflectance across growth stages under the control nitrogen dose 28

5.3 Variation in wheat canopy spectral reflectance across growth stages under the control, underdose and overdose nitrogen 29

5.4 Variation in vegetation indices across growth stages under the control, underdose and overdose nitrogen 31

5.5 Identification of nitrogen stress using UAV based hyperspectral sensor 37
5.6 Comparison of hyperspectral sensor and spectroradiometer measurements . . . 39
5.7 Temporal spectral variation and disease progression in soybean 40

6 CONCLUSION **42**

7 FUTURE WORK **44**

References **45**

List of Figures

1.1 Hyperspectral data cube - a three-dimensional representation of a hyperspectral image. X and Y represent the spatial dimension while the Z dimension shows the spectral information. The spectral information of vegetation and soil pixel is shown at the right of the plot. 12

3.1 The geographical location of the farm that lies in the central part of India 18
3.2 The geographical location of the farm that lies in the central part of India 19

4.1 Growth stage of wheat during the crop cycle 22
4.2 The DJI drone mounted with a hyperspectral camera used for hyperspectral data collection. 22
4.3 The flight plan for UAV-based hyperspectral acquisition covering the experimental site. 23
4.4 (**A**) UAV hyperspectral imagery of the experimental plot. (**B**) masked vegetation using NDVI. 24
4.5 A detailed workflow illustrating the experimental setup and field data collection using multiple sensors, followed by hyperspectral image preprocessing performed in Spectronon software (version 3.4.11), and data analysis in Python (version 3.12.3). 25

5.1 Spectral profiles of vegetation and soil at different processing stages. (**A**) Raw radiance captured using the UAV-based hyperspectral sensor. (**B**) Reflectance spectra obtained after radiance-to-reflectance conversion using a spectrally flat reference panel. (**C**) Smoothed spectra after applying a Savitzky–Golay filter. . 27
5.2 Temporal change in spectra of wheat during the crop cycle for control nitrogen dose. Growth stages shown are (a) CRI (b) tillering (c) booting (d) flowering (e) milking 28

5.3 The Early-stage spectral reflectance variation in control, underdose, and overdose nitrogen treatments, averaged over the subplots with the same treatment. The solid lines represent the mean spectral reflectance, with sample sizes of $n = 12$ for the control and $n = 3$ for both underdose and overdose treatments, while the shaded region represents the 95% confidence interval (CI) around the mean. A clear distinction can be observed for different doses on 7^{th} Feb 2025, 14^{th} Feb 2025, and 28^{th} Feb 2025, whereas at an early stage on 3^{rd} Feb 2025,, no distinction was observed. (**A**) 3^{rd} Feb 2025; (**B**) 7^{th} Feb 2025; (**C**) 14^{th} Feb 2025; (**D**) 28^{th} Feb 2025. 30

5.4 Time series of nitrogen-sensitive vegetation indices in wheat, namely (**A**) NDVI, (**B**) NDRE, (**C**) ND_{705}, (**D**) $CL_{red-edge}$, and (**E**) DATT, in underdose, control, and overdose nitrogen treatments. Overdose treatment increases chlorophyll and canopy density, resulting in higher index values compared to underdose and control. 34

5.5 The p-values for the ANOVA test from pairwise statistical comparisons (control vs. underdose, control vs. overdose, and underdose vs. overdose) across five vegetation indices (NDVI, ND_{705}, NDRE, $CL_{red-edge}$, and DATT) between 30^{th} jan 2025 and 21^{st} March 2025. Cell colour indicates significance level, with blue representing low p-values (highly significant) and dark red representing high p-values (non-significant). The highly significant results ($p < 0.05$) are highlighted in black boxes. 36

5.6 Vegetation index map using UAV-based hyperspectral imagery captured on 17^{th} Feb 2025. 37

5.7 Normalized reflectance spectra obtained from UAV-based hyperspectral imagery for underdose, control, and overdose treatments averaged over subplots with the same nitrogen treatment. The shaded region represents the standard deviation among treatment replicates. 38

5.8 (**A**) Spectral comparison between UAV-based hyperspectral data and handheld spectroradiometer data post irradiance normalisation for the overdose nitrogen treatment, showing strong agreement in terms of Pearson correlation: r = 0.9913. (**B**) Spectral comparison for the underdose nitrogen treatment, also indicating high consistency between both sensors in terms of Pearson correlation: r = 0.9841. 39

5.9 Hyperspectral image of the soybean experimental field showing spatial variability in crop condition across the study area. A) 2^{nd} Aug 2025, B) 6^{th} Aug 2025, C) 12^{th} Aug 2025 40

5.10 Temporal variation in hyperspectral reflectance of soybean canopy on 2^{nd} Aug 2025 (healthy), 6^{th} Aug 2025 (slightly affected), and 12^{th} Aug 2025 (early disease stage). A clear increase in reflectance, particularly in the NIR region, is observed as the disease progresses. 41

Chapter 1

Introduction

Remote sensing makes it possible to get data about any object without having to come into close proximity to it (1). Its implementation is revolutionizing agricultural planning and management. It appears that farm management will advance to the next level of production and productivity with the advent of new technologies. The efficient use of key agricultural resources, such as water, fertilizer and pesticides, when and where needed, can improve agricultural output(2). Remote sensing makes it easier to precisely model crops and monitor these factors in real time. Seasonal patterns in the crop's biological life cycle are followed when assessing crop health. This method makes it possible to precisely and promptly gather data without damaging the crop through sampling. Crop growth, development, nutritional deficiencies, illnesses, moisture stress, water management, and weed control can all be tracked with remote sensing. It can be used to monitor crop growth over a large area and for a range of periods. Understanding how agronomic management and environmental conditions affect crop production is crucial(3).

Wheat (Triticum aestivum) is one of the world's most crucial staple crops that significantly contributes to global food security (4). It provides approximately 20% of global dietary energy and protein intake (5). According to the Food and Agriculture Organisation (FAO), current wheat production is about 750 million tons, whereas the estimated demand by 2050 is over 840 million tons (6). Therefore, it is necessary to maximise agricultural outputs. The quality and production of wheat grain are significantly affected by fertilization. Nitrogen (N) is a crucial nutrient for plant growth and one of the most important nutrients in crop production across all agroecological regions of the world (7). The optimum nitrogen treatment increases the amount of spikes, increases the grains per unit area, improves tiller formation, and encourages canopy development (8). However, both nitrogen underdose and overdose treatments lead to negative physiological and environmental effects. Insufficient N supply reduces the yield by up to 20–30% (9), whereas excessive fertilization implies wasting resources and an increase in environmental pollution (10). The expense of fertilizing wheat with nitrogen can reach up to 30%

of the overall cost of production, and between 50 and 75% of the nitrogen given to the field is lost by leaching into the soil rather than being utilized by the plant (11). Therefore, to maintain high productivity, lower production costs, and minimize environmental contamination, precise monitoring of nitrogen stress is crucial.

Soybean is a major globally traded crop commodity(12). As an important legume and oilseed crop, soybean is widely used for human consumption and animal feed(13). However, abiotic and biotic factors, such as climate change, drought salinity, disease incidence, and insect pests, reduce soybean production(14). Disease incidence, along with other biotic factors, significantly reduces soybean yield and quality, driving research related to disease biology, epidemiology, and effective management practices(15) . Plant pathogens such nematodes, bacteria, viruses, fungi, and phytoplasma infect plants at the pre and post-emergence stages as well as in the later phases of crop growth till maturity. A study reports that pests and diseases cause 20–40% yield losses in most crops worldwide(16). Among various disease-causing factors, yield loss from viral disease in soybeans is hard to predict due to variability in cultivars, virus strain, and the time of infection(17). Viral diseases of soybean, such as yellow mosaic, can reduce yield by up to 85.7% when infection occurs early in plant growth(18). Similarly, another virus, bean pod mottle virus, caused yield loss ranging from 3 to 52% depending on infection severity in the field trial in the United States(19). Reported first in South Korea and North America, the Soybean yellow mottle mosaic virus (SYMMV) belongs to the family Tombusviridae (20). As the name suggests, the symptoms of this viral disease include yellowing, mosaic, mottle, stunting, and leaf rolling(21). Given its highly contagious nature and potential to significantly impact yields, monitoring and accurate identification of SYMMV are crucial for effective disease control and management.

Early disease prediction in crops is important for timely intervention, mitigation, and prevention of wide spread damage. Therefore, crop monitoring and early management of diseases and pests are essential, as accurate diagnosis and detection are key to ensuring optimal yield and good quality(22). Methods of disease identification, such as examination by plant pathologists and visual monitoring, of ten lack accuracy and can be time-consuming(23). Similarly, reliance on visual judgment often leads to misidentification, while laboratory inspection requires more precise instruments, advanced knowledge, and strict operating standards, limiting accessibility and accuracy(24). A variety of sensors are used in remote sensing to capture data. The electromagnetic radiation is detected by these sensors. There are two types of these sensors: active sensors and passive sensors. Radiation released from the Earth's surface or reflected by an item is recorded by passive sensors. Conversely, active sensors—like RADAR and Lidar—emit electromagnetic radiation of their own(25). The majority of sensors used in agricultural remote sensing are made to capture a particular percentage of electromagnetic radiation. Numerous materials can be analyzed both qualitatively and quantitatively using the

electromagnetic spectrum's interaction with the substance (26). Multispectral and hyperspectral imaging are particularly valuable in precision agriculture, allowing the monitoring of plant health, nutrient status, and stress responses. Multispectral sensors capture data in several broad wavelength bands—typically spanning visible, red-edge, and near-infrared regions. In comparison, Hyperspectral sensors record reflectance across numerous, narrowly spaced spectral bands, enabling more precise measurement of subtle plant biochemical and physical traits (27) as shown in Figure 1.1.

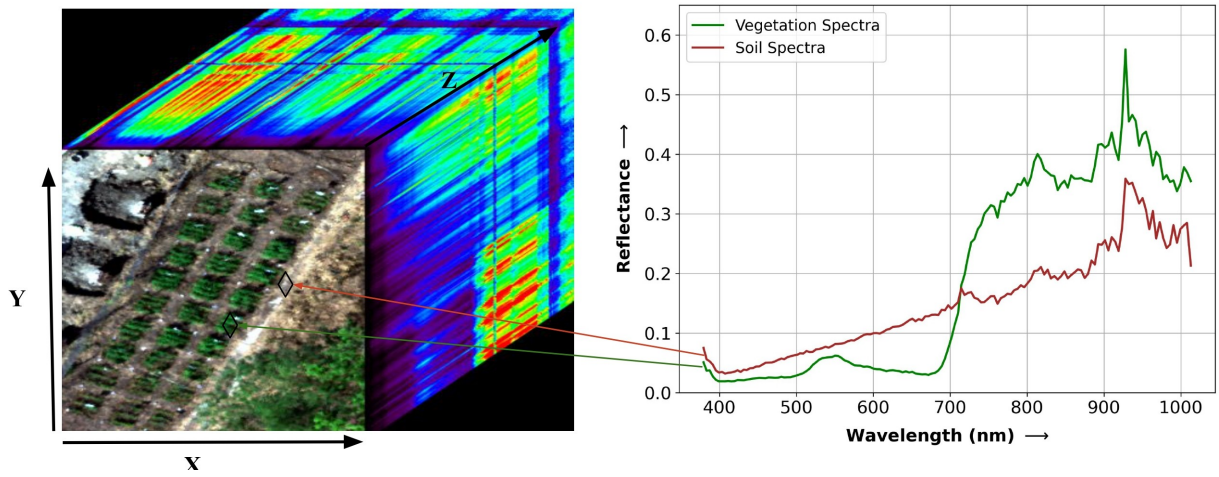


Figure 1.1: Hyperspectral data cube - a three-dimensional representation of a hyperspectral image. X and Y represent the spatial dimension while the Z dimension shows the spectral information. The spectral information of vegetation and soil pixel is shown at the right of the plot.

This higher spectral resolution supports accurate monitoring of chlorophyll, nitrogen status, moisture content, facilitates early identification of nutrient imbalances, diseases, and environmental stresses (28). Furthermore, integrating both multispectral and hyperspectral sensors with UAVs enhances spatial and temporal resolution, making them suitable for detailed field-level monitoring. This combination allows timely, informed agricultural decisions that can optimize input use and boost crop productivity. Therefore, in contemporary agriculture, multispectral and hyperspectral remote sensing greatly increase crop monitoring precision and work in tandem. Satellite-based hyperspectral sensors like Hyperion, CASI, MicroHyperspec, and others record spectral signals in hundreds of narrow bands, enabling accurate detection of crop biochemical parameters like nitrogen and chlorophyll content, and allow large-scale and long-term monitoring, but they offer very coarse spatial resolution and low revisit frequency that limit field-level monitoring. A Unmanned Aerial Vehicle (UAV) based hyperspectral imagery would be preferable to overcome these challenges. A UAV equipped with a hyperspectral sensor offers excellent spatial and spectral resolution, high temporal resolution, ease of use, and access to the data immediately following takeoff. The introduction of hyperspec-

tral UAV sensors with narrow bandwidths revolutionized crop monitoring by enabling precise prediction of plant nitrogen levels and, consequently, estimation of nitrogen stress (29). The widespread use of hyperspectral data for crop parameter acquisition suggests the need to review the progress of research in this field.

Therefore, aerial remote sensing (RS) using drones (Unmanned Aerial Vehicles) (UAV) or Unmanned Aerial Systems (UAS) with intelligent visual systems may be an efficient and inexpensive way for farmers to detect early crop stress and plant diseases in a variety of agricultural fields, from the most intimate greenhouse to the largest farm(30).

1.1 Motivation

By 2050, there will likely be more than 9.7 billion people on the planet, and their food needs could triple. As a result, increasing agricultural productivity is essential. The issues of an expanding population, depleting resources, and inefficiencies in conventional agricultural practices must all be addressed by employing efficient farming practices. Conventional methods for determining and monitoring important crop characteristics include time, extensive sampling, and expensive laboratory chemical analysis, all of which are impractical from an environmental and financial standpoint on a large scale(31). Advanced crop monitoring using multispectral and hyperspectral sensors mounted on unmanned aerial vehicles (UAVs) can enable precise crop monitoring. Soybean feeds billions of people and supports global livestock industries, yet viral diseases yields by up to 85.7% long before a farmer even notices. Early detection of diseases in soybean is crucial to prevent severe yield losses and ensure crop quality. Traditional methods such as visual inspection or laboratory testing, are often time-consuming, subjective and not feasible over large areas. Many diseases become visible only after significant damage has already occurred. Advanced techniques like UAV-based hyperspectral imaging offer a non destructive and efficient way to detect subtle physiological changes in plants before visible symptoms appear. This enables farmers to take targeted and timely action, reducing input costs and improving productivity. Therefore, developing reliable early detection methods is essential for sustainable soybean cultivation and food security.

Chapter 2

Review of Past Work and Problem Formulation

2.1 Literature Review

Many studies demonstrate that UAV-based hyperspectral imaging can flag nitrogen stress up to 2 weeks before visual symptoms. Benincasa et al. improved wheat yield forecast accuracy from 65% to 82% at jointing (32), and Yu et al.'s BES-ELM model ($R^2 = 0.837$) pinpointed rice NNI deficits during vegetative growth (33). Early action based on these detections can reduce nitrate leaching and N_2O emissions by up to 30%, increase nitrogen-use efficiency by about 20%, and increase final yields by 8–12%. Recent advances in hyperspectral remote sensing and unmanned aerial vehicle (UAV) technologies have opened new possibilities for efficient and precise nitrogen stress monitoring. For instance, Tao et al. (2020) utilized UAV-based hyperspectral data to estimate crop growth parameters, demonstrating its effectiveness in assessing crop development (34). Similarly, Moghimi et al. (2019) integrated deep neural networks with UAV hyperspectral imagery to predict high wheat yields (35). Another study examined how well hyperspectral imaging from unmanned aerial vehicles (UAVs) could predict the concentrations of nitrogen (N), phosphorus (P), potassium (K), and sulphur (S) in potato plants (36). Abiotic stressors, like water stress and nutrient shortages, can have a more detrimental effect on crop productivity than biotic stress, which can lower crop yields by 70% (37). So, continuous monitoring of abiotic stress is not just an option, but a requirement for better crop productivity. Previous studies have demonstrated the potential of airborne and UAV-based hyperspectral imagery for assessing nitrogen status in wheat, particularly through red-edge indices and nitrogen-sensitive wavelengths (38; 39; 40). However, these studies have largely focused on quantitative nitrogen estimation at established growth stages, while recent approaches combining spectral and textural information have further improved prediction accuracy (41). Red-edge hyperspectral information has also been successfully used to estimate aerial nitrogen uptake in

winter wheat (42). Despite these advances, limited attention has been given to the early spectral discrimination of contrasting nitrogen treatments before visible canopy symptoms become pronounced. The present study addresses this gap by analysing the complete hyperspectral response of wheat at an early growth stage, identifying nitrogen-sensitive wavelength regions, and applying statistical and spectral analyses to quantify treatment discrimination. The integration of UAV hyperspectral data with ground-based spectroradiometer observations further strengthens the validation of the results. Thus, this study extends previous work from nitrogen estimation toward early and statistically validated nitrogen-treatment discrimination. Several studies have demonstrated the effectiveness of UAV-based hyperspectral imaging for early crop disease detection. Guo et al. (2024) proposed a framework integrating canopy pigments and spectral indices from UAV hyperspectral data for early stripe rust detection in wheat, achieving 78.1% accuracy during the asymptomatic phase using a Random Forest model, with pigment parameters found to be more discriminative than spectral indices alone(43). Advancing beyond classification, Zhang et al. (2023) developed an end-to-end deep learning approach for pixel-level quantitative regression of the wheat stripe rust Disease Index from UAV hyperspectral imagery acquired over 1,000 wheat varieties, enabling continuous severity mapping rather than binary disease labeling(44). Abdulridha et al. (2020) validated both UAV-based and benchtop hyperspectral systems for simultaneous detection of target spot and bacterial spot in tomato, demonstrating that machine learning classifiers could reliably distinguish multiple disease types across field and laboratory scales(45). While previous studies have demonstrated the potential of hyperspectral imaging for soybean disease detection, existing works remain largely confined to benchtop or greenhouse setups with detached leaf samples under controlled illumination conditions limiting their direct applicability to real-world field environments(46). Furthermore, UAV-based hyperspectral studies in soybean have exclusively targeted soilborne fungal diseases such as Sudden Death Syndrome (SDS)(47), and no study has yet extended this approach to viral pathogens at the canopy scale. To address this critical gap, this letter presents, to the best of the authors' knowledge, the first investigation into early-stage detection of Soybean Mosaic Virus (SMV) using UAV-mounted hyperspectral imaging under actual field conditions, bridging the scale gap between controlled laboratory studies and operational precision agriculture deployment.

2.2 Problem formulation for early stage nitrogen stress detection in wheat

As presented above, many studies have been performed for nutrient stress monitoring, but very limited successful studies have been conducted for early-stage nitrogen stress monitoring. This study proposes detecting nitrogen stress at an early stage in wheat using UAV-based hyperspectral data, a handheld spectroradiometer, and an NDVI sensor. The major topic of this work is how to use a hyperspectral-equipped UAV and in situ measurements with a variety of tools, such as a handheld spectro-radiometer, multispectral camera, NDVI sensor, soil moisture sensor and thermal camera to monitor and evaluate abiotic stress. The study seeks to detect early nitrogen stress in wheat by evaluating:

(A) Variation in wheat canopy spectral reflectance across growth stages under the control nitrogen dose.

(B) Variation in wheat canopy spectral reflectance across growth stages under the control, underdose and overdose nitrogen.

(C) Variation in vegetation indices across growth stages under the control, underdose and overdose nitrogen.

(D) Identification of Nitrogen stress Using UAV-based hyperspectral sensor data.

(E) Comparison of UAV based data and spectroradiometer data for different nitrogen treatments.

2.3 Problem formulation for early soybean disease detection

In this study, we address this challenge by utilizing three categories of hyperspectral datasets: (i) healthy plants, (ii) less healthy plants, and (iii) plants exhibiting early visible symptoms. The core objective is to investigate whether subtle spectral variations across these categories can be used to detect disease onset before it becomes visually prominent. By analyzing differences in spectral reflectance patterns and validating them with field observations, the study aims to establish a reliable approach for early-stage disease detection.

Chapter 3

Study Area

3.1 Study area of wheat

This study was conducted at IIT, Indore in Indore district in western Madhya Pradesh (MP), India and covers an area of about 3898 km2 located between 75.5^0 E to 76.2^0 E longitude and 22^0 N to 23.10^0 N latitude. MP has a continental climate, with minimum, maximum, and average temperatures of 8.10^0 C, 43.2^0 C and 26^0 C, respectively. The study site is shown in Figure 3.1. MP is the third largest producer of wheat in India. In this region, wheat, potato, and onion are grown during October-April cycle and typically harvested in mid-March or early-April. Soil quality, monsoon variation, and heat stress affect crop growth. The presence of black clayey soil rich in nutrients like iron, magnesium, etc., is beneficial for flourishing dry crops(48). The topography of this region is mainly flat, with slightly higher terrain in the southwest direction.

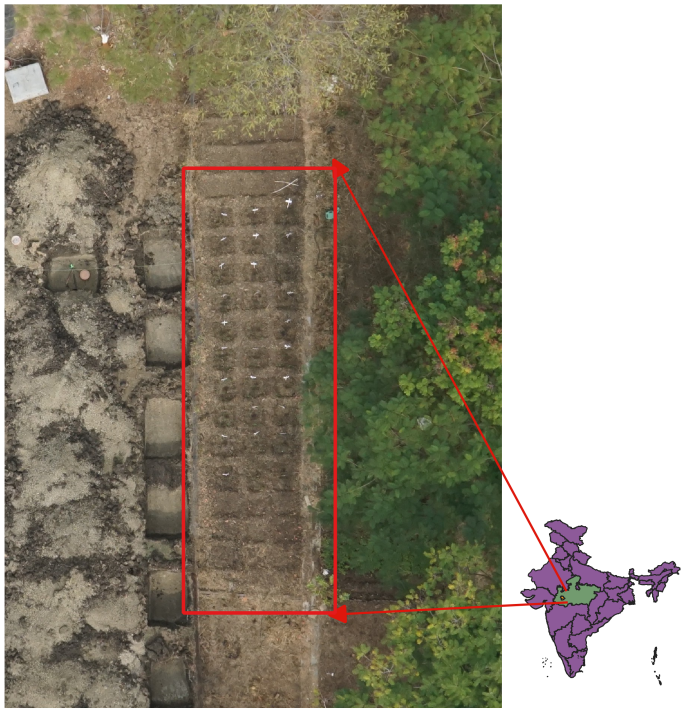


Figure 3.1: The geographical location of the farm that lies in the central part of India

3.2 Study area of soybean

The study was conducted in an experimental agricultural field located near Indian Institute of Technology Indore, Indore Madhya, Pradesh. The region lies between 22°N latitude and 76°E longitude and is characterized by a subtropical climate with hot summers, moderate monsoon rainfall and mild winters. The average annual temperature ranges from about 8°C in winter to 43°C in summer, with most rainfall occurring during the monsoon season typically between June to September. A detailed map of the study area showing the field location and surrounding region is presented in Figure 3.2.

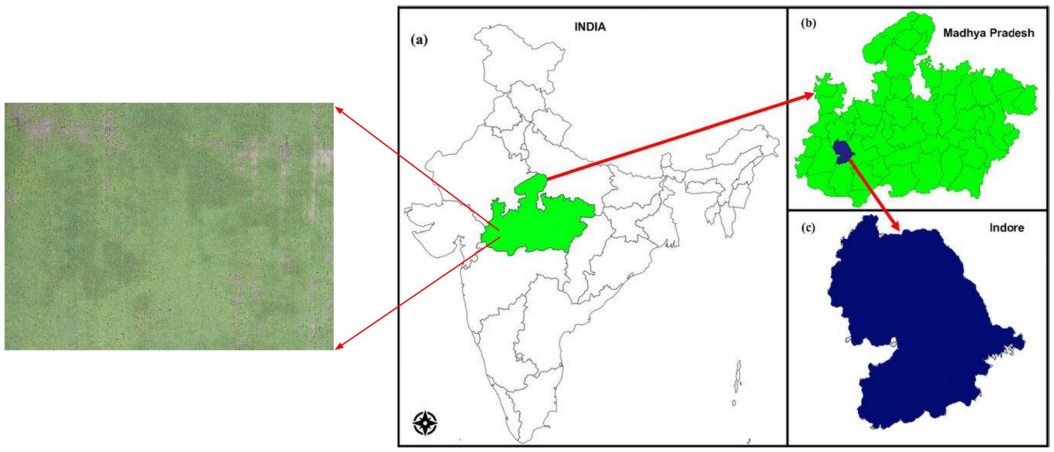


Figure 3.2: The geographical location of the farm that lies in the central part of India

Chapter 4

MATERIAL AND METHOD

4.1 Field data

The field data for this study were collected through carefully controlled experimental conditions. The experiment was conducted by establishing 30 subplots, each measuring 3×3 feet, within the experimental farm. Each subplot was sown with the wheat variety HI-1544, using a total of 527 grams of seeds. On average, approximately 17.5 grams of seeds were sown per subplot. Sowing operations were carried out manually on 3^{rd} Jan 2025 to ensure uniform seed distribution across all subplots. A total of eight irrigation events were conducted throughout the growing season, some of which are shown in Figure 4.1 and labelled as I1, I2, etc. beginning with the first irrigation on 5^{th} Jan 2025, just two days after sowing, and then approximately every 10 days, irrigation was done .

Fertilization was similarly managed in a structured manner. Three fertilization rounds were conducted during the crop cycle. The first fertilization took place on 9^{th} Jan 2025, coinciding with early crop establishment. The second fertilization was applied on 30^{th} Jan 2025, targeting the crop's vegetative growth phase. The final application was made on 17^{th} Feb 2025, to support the reproductive development stage. Fertilizer doses were administered based on specific treatment plans to induce nutrient stress or optimize crop nutrition, depending on the experimental group.

To study the effects of nutrient and water variations, the subplots were divided into three main treatment categories recommended by Indian Council of Agriculture Research (ICAR):

1)**Nitrogen Treatments:**

A) Recommended nitrogen dose (120 kg/ha)

B) Nitrogen underdose (60 kg/ha)

C) Nitrogen overdose (180 kg/ha)

2)**Phosphorus/Potassium (P/K) Treatments:**

A) Recommended P/K dose (60 kg/ha and 30 kg/ha)

B) PK underdose (30 kg/ha and 15 kg/ha)

C) PK overdose (90 kg/ha and 45 kg/ha)

3) **Water Treatments:**

A) Control (recommended irrigation volume)

B) Water underdose (50% less than Control)

C) Water overdose (50% more than Control)

These treatments were implemented to systematically induce varying levels of abiotic stress, allowing for the observation and analysis of crop physiological and spectral responses under different nutrient and water regimes.

For the in situ data, multiple sensors and imaging devices were used to capture detailed biophysical and spectral information. A handheld Apogee PS-100 spectroradiometer having a wavelength range of 350-1000nm was used to record canopy reflectance across a continuous spectral range, critical for hyperspectral analysis. Soil moisture content was monitored using a 5 probe soil moisture sensor, enabling real-time assessment of water availability within the root zone.

Vegetative vigor was assessed using a dedicated NDVI sensor, which provided normalized difference vegetation index measurements directly in the field. Thermal imaging was performed with a thermal camera to detect canopy temperature variations, offering indirect insights into plant water status and stress levels. Multispectral images were captured using a multispectral camera (Parrot Sequoia). Four discrete spectral bands, namely green, NIR, red, and red-edge, supplemented the hyperspectral data with spatially resolved spectral information. Additionally, a DSLR camera was used for high-resolution RGB imagery collection to document crop morphology and growth stages visually. The details of instruments are shown in Table 4.1.

Table 4.1: Detail of Instruments used for Data Acquisition

Data	**Instrument Used**	**Specification**	**Use Case**
Spectral Signature	Apogee PS-100 Spectroradiometer	350-1000 nm	Indices
Hyperspectral UAV Images	DJI Matrice 300 RTK (Drone)	Range (vertical): 300 m	To Mount Hyperspectral Sensor
RGB Aerial Imagery	Ideaforge UAV	SONY ILCE-5100 RGB camera	Initial Aerial Monitoring
NDVI	Apogee NDVI Sensor	Downward looking	NDVI Validation

All sensors were carefully calibrated following manufacturer guidelines before and during

field campaigns to ensure data accuracy and reliability. Data collection was performed under clear sky conditions, predominantly between 01:00 PM and 04:00 PM, to minimize variations due to solar zenith angle changes and atmospheric effects. The field condition and the experimental setup is shown in Figure 4.1.



Figure 4.1: Growth stage of wheat during the crop cycle

4.2 UAV data

In addition to in situ measurements, aerial hyperspectral imagery was captured using a Resonon Pika L hyperspectral sensor(Resonon Inc., Bozeman, MT, USA) having a 400–1000 nm spectral range, 281 spectral channels, and a 2.7 nm (FWHM) spectral resolution, mounted on a DJI Quadcopter (DJI, Shenzhen, China) as shown in Figure 4.2.



Figure 4.2: The DJI drone mounted with a hyperspectral camera used for hyperspectral data collection.

Before UAV data collection, a detailed flight plan was prepared based on the required flight altitude, desired spatial resolution, target area coverage, and prevailing illumination conditions (Figure 4.3). The UAV missions were pre-planned using the Resonon Ground Station v7.13 desktop application. A constant takeoff and flight altitude of 50 m was maintained, resulting in a ground sampling distance (GSD) of 0.63 cm/pixel. The takeoff speed was set to 10 m/s, while the survey flight speed was maintained at 1 m/s to ensure high-quality data acquisition. The flight path was designed with a course angle of 29°. The flight altitude was kept constant (50 m) in order to maintain uniformity in data collection. The data was collected under clear-sky conditions, preferably between 1:00 PM and 4:00 PM to avoid the shadow effect at peak noon. The solar zenith angle was 36.5°, while the wind speed was 5.9 km/h during the data acquisation. Pre-planned flight paths ensured consistent coverage and 70% to 80% overlap between successive images. The hyperspectral image of the experimental plot and the corresponding NDVI masked vegetation is shown in Figure 4.4. NDVI thresholding was applied to mask soil pixels from vegetation. A threshold value of 0.3 was adopted, as pixels with NDVI below this value were considered non-vegetated, following common practice in crop remote sensing studies (49). Together, UAV-based hyperspectral and spectroradiometer datasets provided rich spatial and spectral information, enhancing the ability to detect subtle variations in plant health, canopy structure, and stress symptoms. The integration of UAV data with ground-collected measurements created a comprehensive, multi-source dataset that significantly improved the monitoring and evaluation of wheat crop responses under varying nutrient treatments.

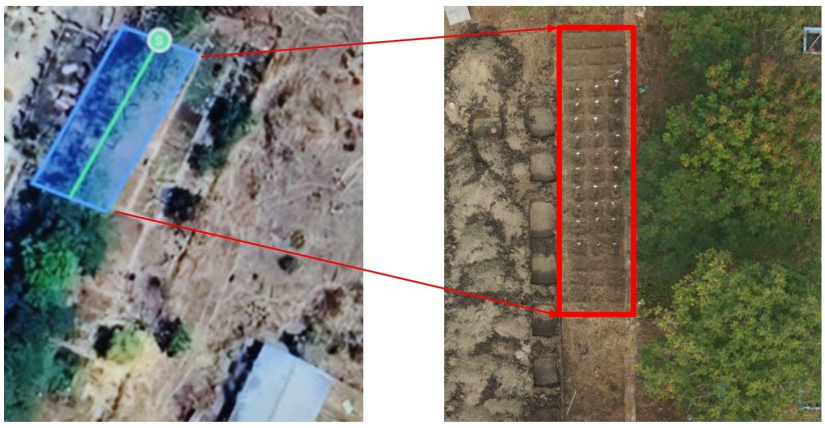


Figure 4.3: The flight plan for UAV-based hyperspectral acquisition covering the experimental site.

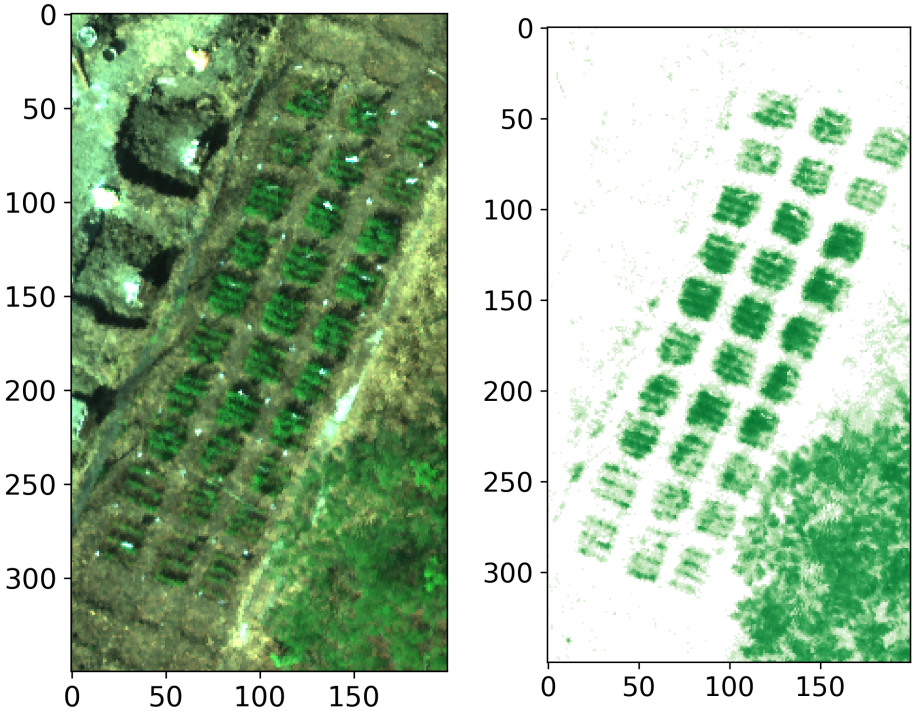


Figure 4.4: (**A**) UAV hyperspectral imagery of the experimental plot. (**B**) masked vegetation using NDVI.

4.3 A detailed workflow

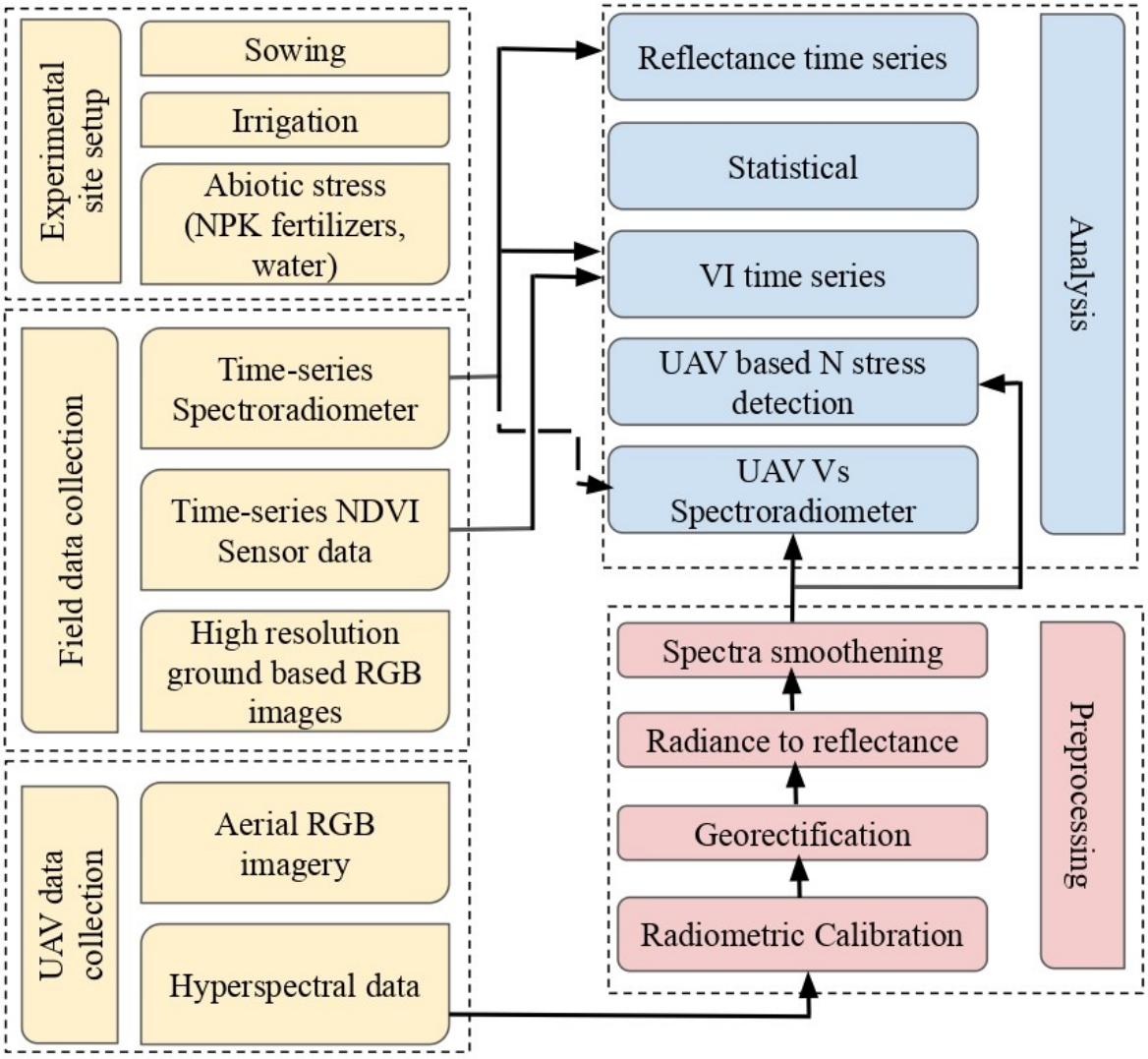


Figure 4.5: A detailed workflow illustrating the experimental setup and field data collection using multiple sensors, followed by hyperspectral image preprocessing performed in Spectronon software (version 3.4.11), and data analysis in Python (version 3.12.3).

Chapter 5

RESULTS AND DISCUSSION

5.1 Preprocessing of hyperspectral data

Preprocessing of hyperspectral imagery for illumination variation, geocoding, and spec- tral calibration was performed in Spectronon Pro software (version 3.4.11). Initially, the flight computer converted the sensor's raw DN values to radiance in real time using a manufacturer-supplied calibration file (radiometric calibration). This ensures that all data cubes generated by the sensor are in radiance units. Following this, the radiance data cubes were processed using the Georectify plugin in Spectronon Pro, designed explicitly by Resonon for georectification. The software allows for the incorporation of a digital terrain model to enhance the georectification accuracy. Subsequently, the georectified radiance values were converted to reflectance. This was accomplished by referencing targets with known reflectivity placed within the study field, featuring a tarp of differing grey levels that reflect 24% and 36% across all spectral bands. To reduce noise in the data, the spectral reflectance curves were then smoothed using a Savitzky–Golay filter (Spectronon Pro software) [38]. For our study, we employed a filter with a kernel size of 13 and a polynomial order of 3, following recommendations provided by the sensor manufacturer. An example of the raw data and preprocessing is shown in Figure 5.1.

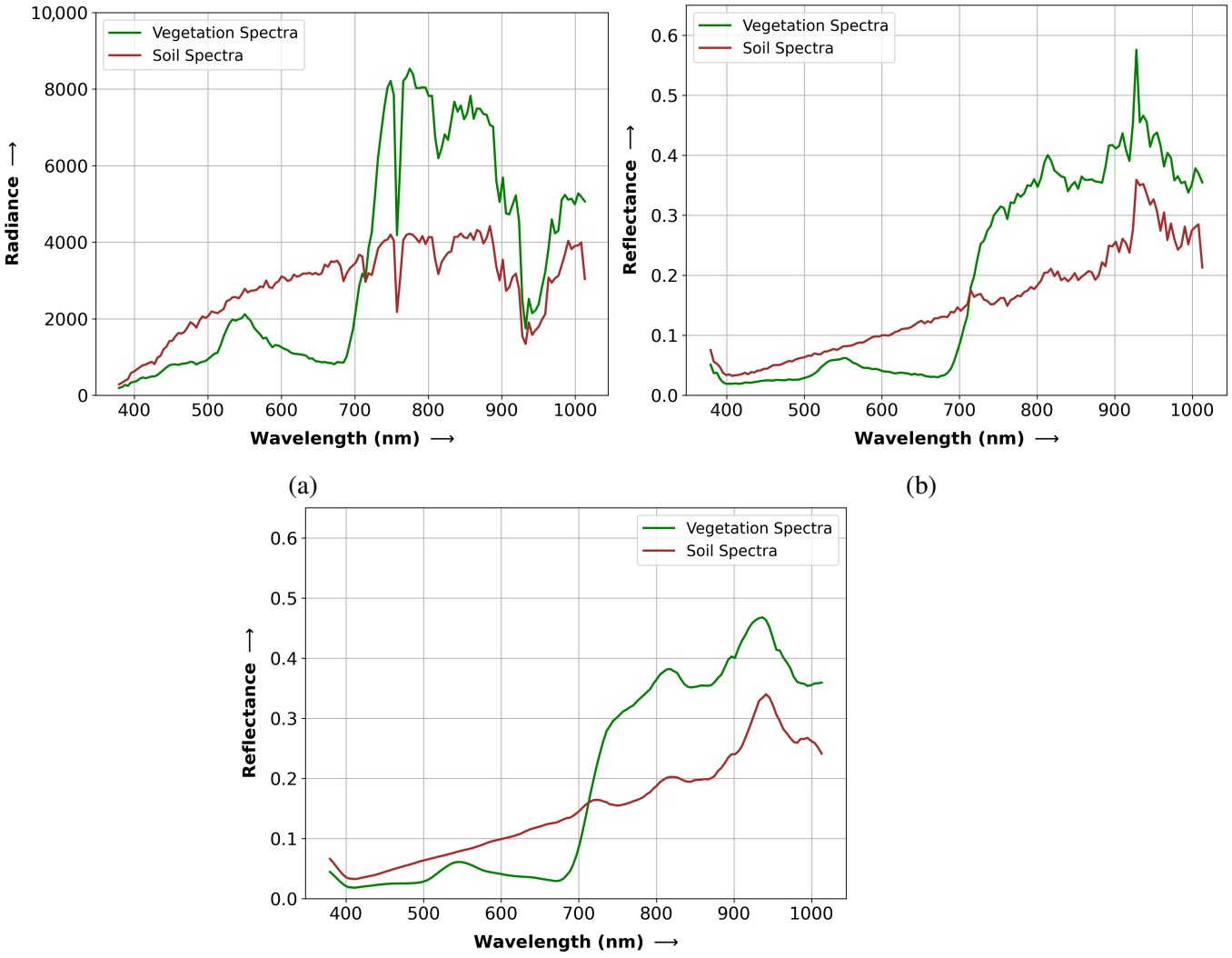


Figure 5.1: Spectral profiles of vegetation and soil at different processing stages. (**A**) Raw radiance captured using the UAV-based hyperspectral sensor. (**B**) Reflectance spectra obtained after radiance-to-reflectance conversion using a spectrally flat reference panel. (**C**) Smoothed spectra after applying a Savitzky–Golay filter.

5.2 Variation in wheat canopy spectral reflectance across growth stages under the control nitrogen dose

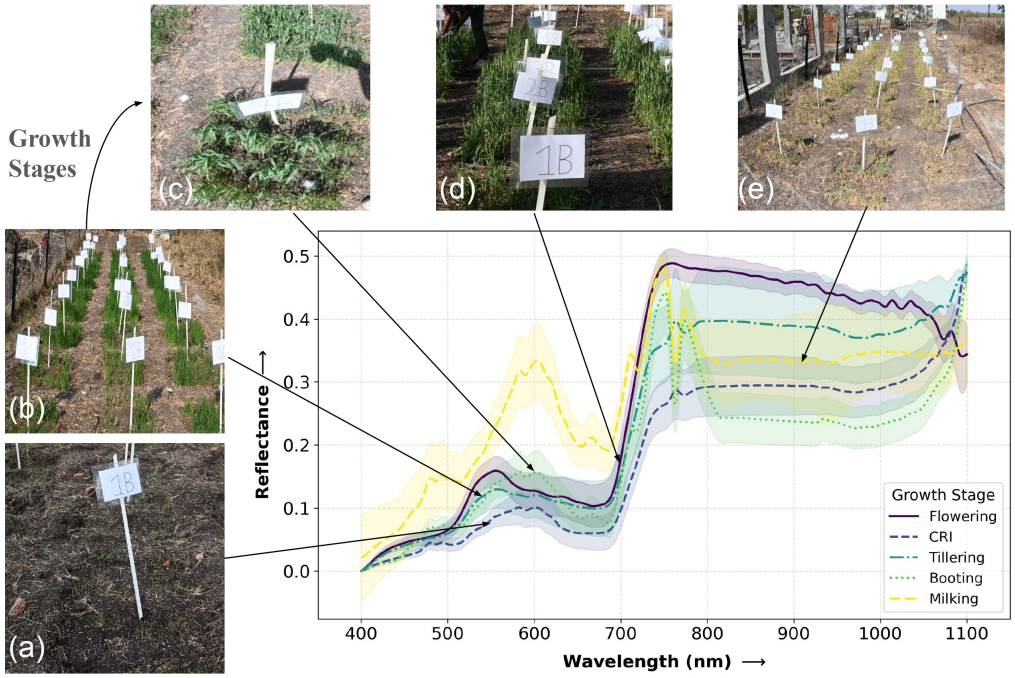


Figure 5.2: Temporal change in spectra of wheat during the crop cycle for control nitrogen dose. Growth stages shown are (a) CRI (b) tillering (c) booting (d) flowering (e) milking

Figure 5.2 represents the reflectance curve for critical growth stages of wheat—Crown Root Initiation (CRI), tillering, booting, flowering, and milking—averaged over all the control subplots. At the CRI stage, reflectance remains the lowest across the entire spectrum, with NIR values ranging approximately from 0.1 to 0.5, as most of the reflectance came from a very small canopy. As the crop reaches the tillering and booting stages, a "green peak" emerges near 550 nm, with reflectance between 0.12 and 0.15 due to increased chlorophyll, while a sharp "red-edge" transition occurs at 700 nm. As the crop reaches the flowering stage, the NIR reflectance reaches its maximum values of approximately 0.5 between 750 and 850 nm, indicating dense canopy closure and complex internal leaf scattering. In the milking stage, a shift is observed: the reflectance in the visible region (500–700 nm) nearly triples, peaking at 0.32 near 600 nm as chlorophyll degrades. Concurrently, the NIR reflectance drops to 0.35, indicating a loss of leaf transition and moisture as the wheat matures and reaches senescence (50). The progression observed in our plots matches the changes in the reflectance curves and reflects the crop's natural physiological development.

5.3 Variation in wheat canopy spectral reflectance across growth stages under the control, underdose and overdose nitrogen

Here, we monitored the variation in spectral reflectance for four growth stages with BBCH code 21 (emergence), 28 (tillering), 33 (stem elongation), and 55 (heading) on the dates 3^{rd} Feb 2025, 7^{th} Feb 2025, 14^{th} Feb 2025, and 28^{th} Feb 2025, respectively. Initially, little variation in reflectance was observed among the N treatments, averaged across subplots with the same treatment. The NIR reflectance (800 to 1000 nm) saturates around 0.35 for all three N treatments, as shown in Figure 5.3A. This indicates that, at this very early stage, the impact of different nitrogen doses has not yet significantly altered chlorophyll concentration or canopy structure enough to detect differences between doses. On 7^{th} Feb 2025, a clear difference can be observed between the control and underdose treatment, particularly in the NIR region, but overdose cannot be differentiated from underdose, as shown in Figure 5.3B. On 14^{th} Feb 2025, the overdose treatment showed the lowest visible reflectance (0.18 at 550 nm), indicating higher chlorophyll-induced absorption, whereas the control treatments showed higher NIR reflectance (0.62–0.4), as shown in Figure 5.3C. On 28^{th} Feb 2025, a clear difference in the visible reflectance spectra of all three doses can be observed. Overdose treatment showed the lowest visible reflectance (0.25), while underdose treatment showed significantly higher visible reflectance (0.3), as shown in Figure 5.3D. These results underscore the potential for spectral monitoring to identify nitrogen stress in its early vegetative phases, providing a data-driven basis for nitrogen management. Spectral reflectance signatures change clearly with the nitrogen level in wheat, and this pattern becomes more visible as the crop grows (51). Only a few studies have shown how canopy reflectance changes across the entire growing season in overdose, underdose, and control nitrogen conditions, even though this information is very important for detecting nitrogen stress at early stages (52). Among the observation dates, 28^{th} Feb 2025 showed the clearest spectral separation among the three nitrogen treatments, particularly in the visible and red-edge regions. Therefore, this date was further examined to identify the specific wavelengths that provided maximum discrimination among the nitrogen treatments. The spectral analysis for 28^{th} Feb 2025 showed that the red to red-edge region (642.4–706.0 nm) had the highest sensitivity to nitrogen variation. Specific sensitive wavelengths were identified at 642.4, 646.6, 650.8, 655.0, 659.2, 663.5, 667.7, 672.0, 676.2, 680.5, 684.7, 689.0, 693.2, 697.5, 701.7, and 706.0 nm. These wavelengths were associated with changes in chlorophyll-related spectral absorption caused by different nitrogen levels. The corresponding analysis highlights the spectral region that provided the greatest discrimination among the nitrogen treatments.

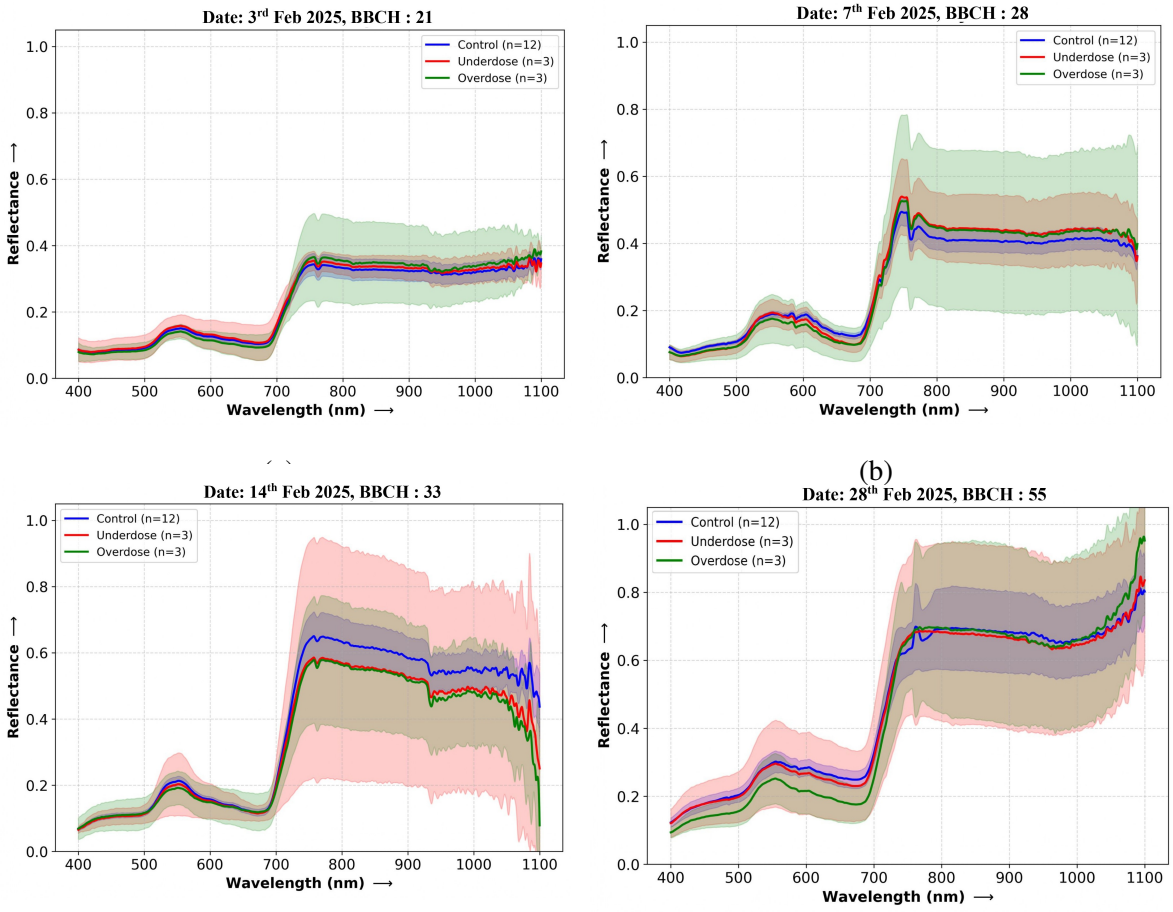


Figure 5.3: The Early-stage spectral reflectance variation in control, underdose, and overdose nitrogen treatments, averaged over the subplots with the same treatment. The solid lines represent the mean spectral reflectance, with sample sizes of $n = 12$ for the control and $n = 3$ for both underdose and overdose treatments, while the shaded region represents the 95% confidence interval (CI) around the mean. A clear distinction can be observed for different doses on 7^{th} Feb 2025, 14^{th} Feb 2025, and 28^{th} Feb 2025, whereas at an early stage on 3^{rd} Feb 2025,, no distinction was observed. (**A**) 3^{rd} Feb 2025; (**B**) 7^{th} Feb 2025; (**C**) 14^{th} Feb 2025; (**D**) 28^{th} Feb 2025.

5.4 Variation in vegetation indices across growth stages under the control, underdose and overdose nitrogen

During the early growth stages, all indices exhibited minimal separation among treatments due to limited leaf area, weak pigment differentiation, and strong soil background influence. On 11^{th} Feb 2025, the overdose treatment achieved the highest index values with the NDVI and $CL_{red-edge}$ peaking at approximately 0.80, and other indices the NDRE, ND_{705}, and DATT—peaking between 0.4 and 0.6. In the overdose treatment, all the vegetation indices have higher values compared to underdose and control, as shown in Figure 5.3. To statistically validate the observed spectral differences between treatment groups, a one-way Analysis of Variance (ANOVA) was performed independently for each vegetation index across twelve acquisition dates, with treatment group (Control, Underdose and Overdose) as the single independent factor and degrees of freedom df=(2,n-3). ANOVA compares the variation between treatment means with the variation within treatments, with $p < 0.05$ considered statistically significant. The initial pairwise p-value heatmaps showed that significant differences between treatment groups occurred only on specific acquisition dates rather than consistently throughout the growing season Figure 5.5. In particular, the Control–Underdose comparison showed significant differences for NDVI ($p = 0.001$) and ND705 ($p = 0.017$) on 3^{rd} Feb 2025, whereas the Control–Overdose comparison showed significant differences for NDVI ($p = 0.023$), ND705 ($p = 0.007$), NDRE ($p = 0.043$), and DATT ($p = 0.045$) on 28^{th} Feb 2025. The assumptions underlying ANOVA were subsequently assessed using the Shapiro–Wilk test for normality and Levene's test for homogeneity of variance. For date $\times$ index combinations showing significant overall ANOVA results, Tukey's HSD post-hoc test was applied to identify the specific treatment pairs responsible for the observed differences. Across the 60 date × vegetation-index combinations, nominally significant ANOVA effects were observed for NDRE and $CL_{red-edge}$ on 7^{th} Feb 2025 and ND705 on 28^{th} Feb 2025. Tukey's HSD indicated that these differences were primarily associated with the Control–Overdose comparison, while comparisons involving the Underdose treatment were not significant. The corresponding ($n^2 = 0.347^{\smile}0.374$) and ($w^2 = 0.249^{\smile}0.272$) values indicated appreciable treatment-associated effects for these date-specific observations as shown in Table 5.2. Overall, the results indicate that nitrogen treatment produced detectable spectral differences at specific stages of crop development, particularly between the Control and Overdose treatments, but these effects were not consistently significant across the complete observation period after accounting for multiple testing. A clear distinction is also evident in the vegetation index map, as shown in Figure 5.6. These results confirm that hyperspectral vegetation indices, particularly those derived from the red-edge region, are reliable indicators of nitrogen status once sufficient canopy structure and pigment development are present, and these findings are very useful in early nitrogen stress detection and also support

pure reflectance behaviour in control, underdose, and overdose nitrogen treatments.

Table 5.1: Vegetation Indices Used for Leaf Nitrogen Estimation

Index Formula	**Short Form**	**Full Form**	**Reference**
NDVI=$\frac{NIR - Red}{NIR + Red}$	NDVI	Normalized Difference Vegetation Index	Tucker, C.J. (1979), *Remote Sensing of Environment*.
NDRE=$\frac{NIR - RE}{NIR + RE}$	NDRE	Normalized Difference Red-Edge Index	Barnes, E.M. et al. (2000), *Precision Agriculture Conference*.
ND_{705}=$\frac{R_{750} - R_{705}}{R_{750} + R_{705}}$	ND_{705}	Red-Edge Normalized Difference 705 Index	Gitelson, A.A. & Merzlyak, M.N. (1994), *RSE*.
CL_{RE}=$\frac{R_{750}}{R_{710}}$	$CL_{red-edge}$	Chlorophyll Red-Edge Ratio Index	Clevers, J. & Gitelson, A. (2013), *IEEE JSTARS*.
DATT=$\frac{R_{740} - R_{720}}{R_{740} + R_{720}}$	DATT	Double-Angle Transformed Triangular Index	Delegido, J. et al. (2011), *Agric. Forest Meteorology*.

Such early stage insensitivity, particularly evident in NDVI is consistent with previous findings showing that incomplete canopy closure and low chlorophyll content diminish nitrogen related spectral contrasts(53). As the wheat crop advanced into booting, flowering and grain filling phases, the spectral response increasingly diverged across the nitrogen levels. In the overdose treatment all vegetation indices have higher values compared with the underdose and control treatments. These results confirm that hyperspectral vegetation indices, particularly those derived from the red edge region are reliable indicators of nitrogen status once sufficient canopy structure and pigment development are present and these finding are very useful in early nitrogen stress detection and also supporting pure reflectance behaviour in control, underdose and overdose nitrogen treatments.

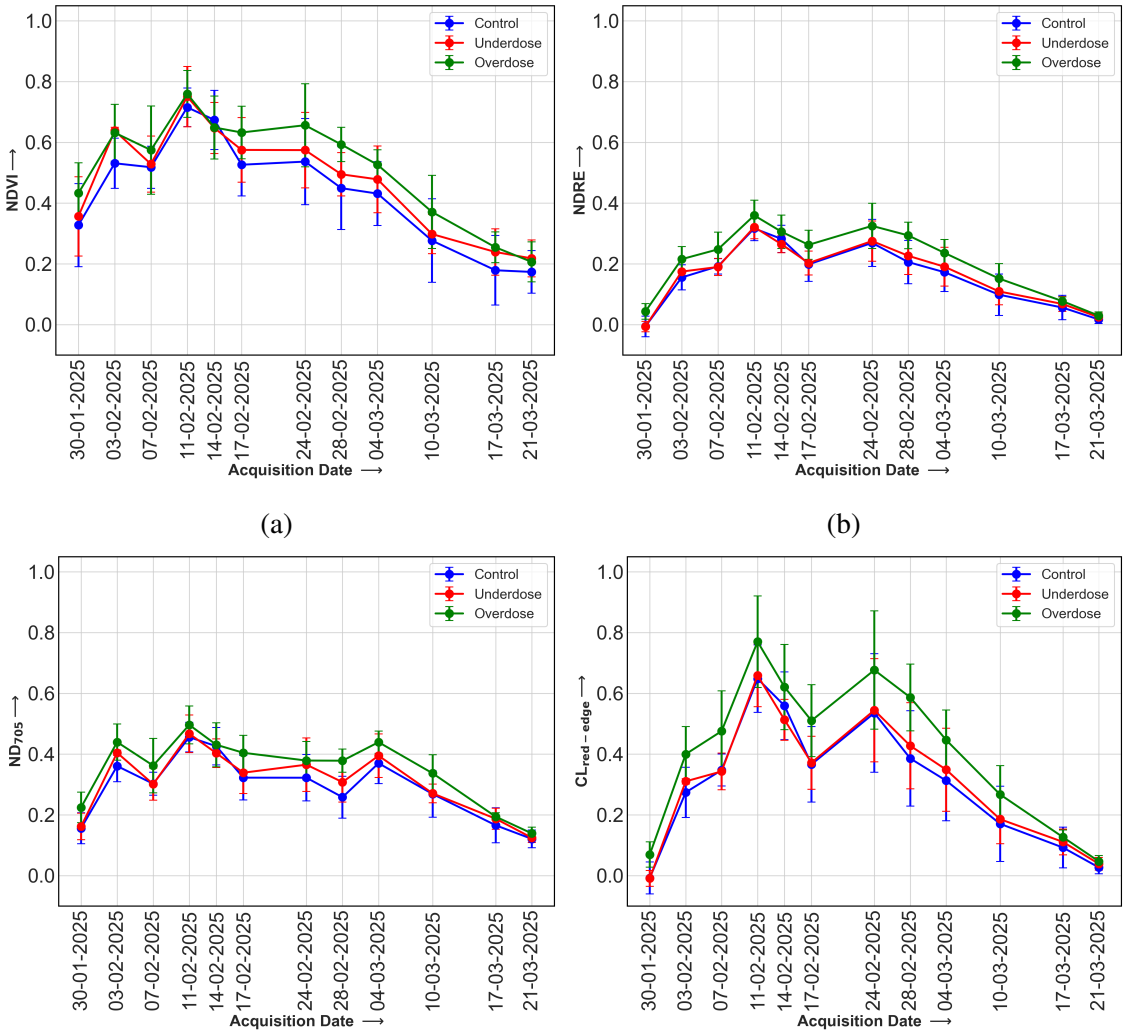
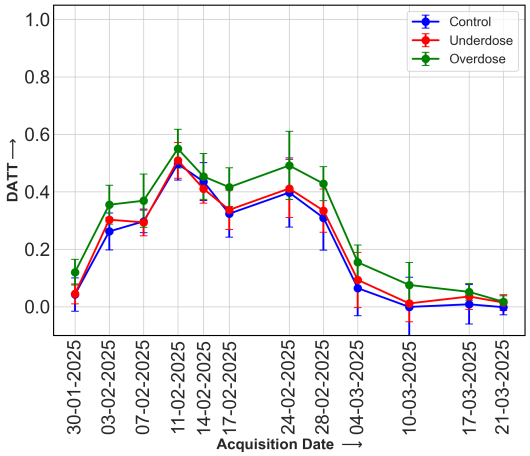


Figure 5.4: Time series of nitrogen-sensitive vegetation indices in wheat, namely (**A**) NDVI, (**B**) NDRE, (**C**) ND_{705}, (**D**) $CL_{red-edge}$, and (**E**) DATT, in underdose, control, and overdose nitrogen treatments. Overdose treatment increases chlorophyll and canopy density, resulting in higher index values compared to underdose and control.



(e)

Table 5.2: ANOVA test statistics, effect sizes, and significant Tukey's HSD comparisons for vegetation indices under different nitrogen treatments.

Date	**Index**	F	η^2	ω^2	**Tukey HSD comparison**
7 Feb 2025	NDRE	3.980	0.347	0.249	Control–Overdose
7 Feb 2025	$\mathrm{CI}_{\mathrm{red-edge}}$	4.313	0.365	0.269	Control–Overdose
28 Feb 2025	ND705	4.178	0.374	0.272	Control–Overdose

F: F-statistic; η^2: eta-squared; ω^2: omega-squared.

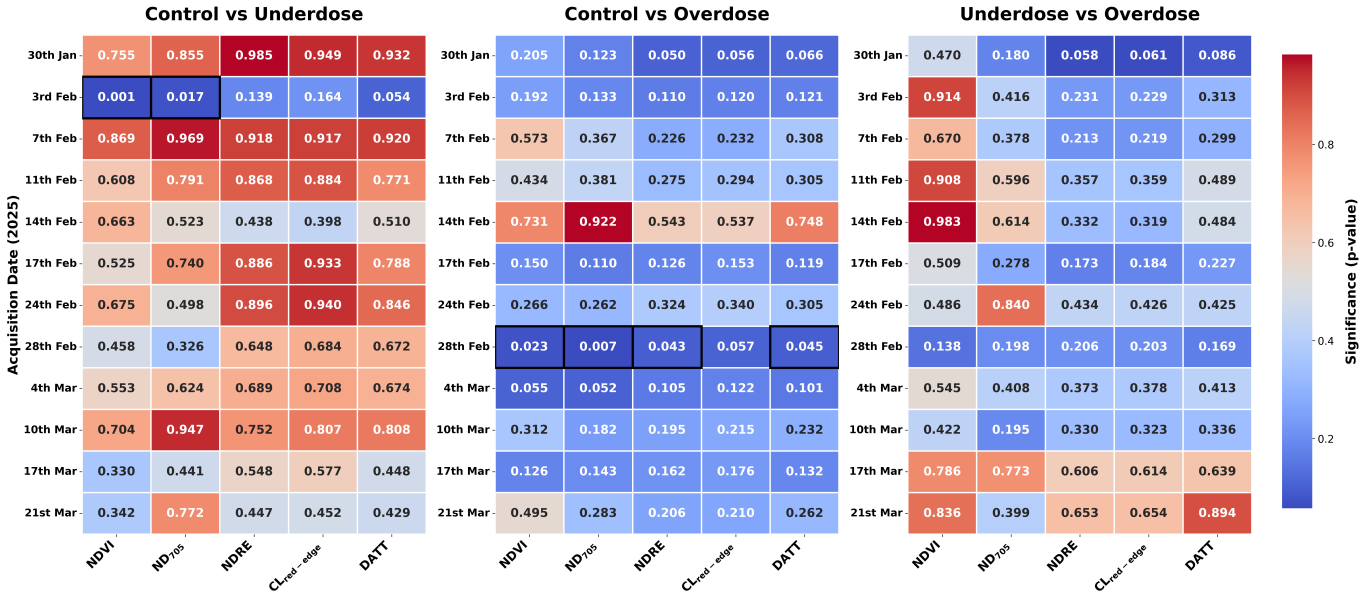


Figure 5.5: The p-values for the ANOVA test from pairwise statistical comparisons (control vs. underdose, control vs. overdose, and underdose vs. overdose) across five vegetation indices (NDVI, ND_{705}, NDRE, $CL_{red-edge}$, and DATT) between 30^{th} jan 2025 and 21^{st} March 2025. Cell colour indicates significance level, with blue representing low p-values (highly significant) and dark red representing high p-values (non-significant). The highly significant results ($p < 0.05$) are highlighted in black boxes.

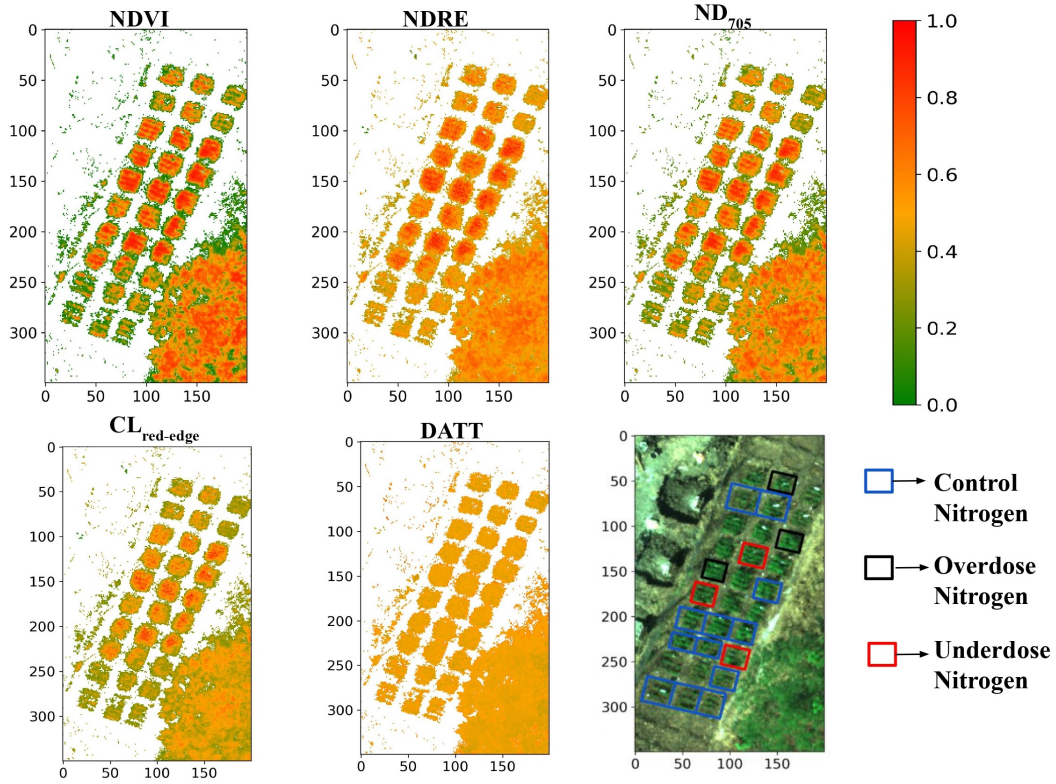


Figure 5.6: Vegetation index map using UAV-based hyperspectral imagery captured on 17^{th} Feb 2025.

5.5 Identification of nitrogen stress using UAV based hyperspectral sensor

For large-scale field monitoring, detecting abiotic stress with a handheld spectroradiometer is time-consuming and operationally challenging. These limitations can be effectively addressed using a UAV-based hyperspectral sensor, which produces results consistent with those of the spectroradiometer. Figure 5.7 represents the spectral reflectance curve averaged over the subplots with the same nitrogen treatment. The underdosed plant canopy showed higher visible-region (400–700 nm) reflectance (0.08–0.11) due to reduced chlorophyll content. Reduced chlorophyll leads to lower absorption at the green wavelength, resulting in higher reflectance (54). In overdose plants, higher chlorophyll content increases radiation absorption in the green region and is associated with greater biomass and canopy development, resulting in lower reflectance (55). The red-edge position shifts toward shorter wavelengths under nitrogen deficiency, a known physiological response that serves as a key indicator of early stress detection (56). For the NIR spectrum, the overdosed plant showed a higher peak (0.42–0.55) due to higher canopy structure, and the underdosed plant showed a peak at a lower reflectance value

(0.3–0.38) due to lesser vegetation canopy. The control-dose plants showed a reflectance value between the overdose and underdose. These findings align with previous research demonstrating the potential of hyperspectral sensors in quantifying nitrogen variability across agricultural plots. This capability is vital for optimizing nutrient management and improving nitrogen use efficiency in wheat cropping systems.

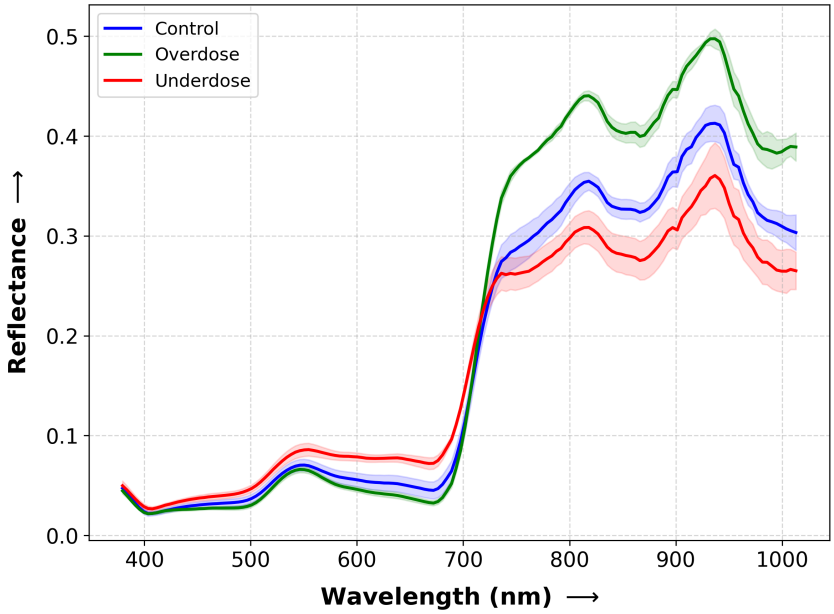
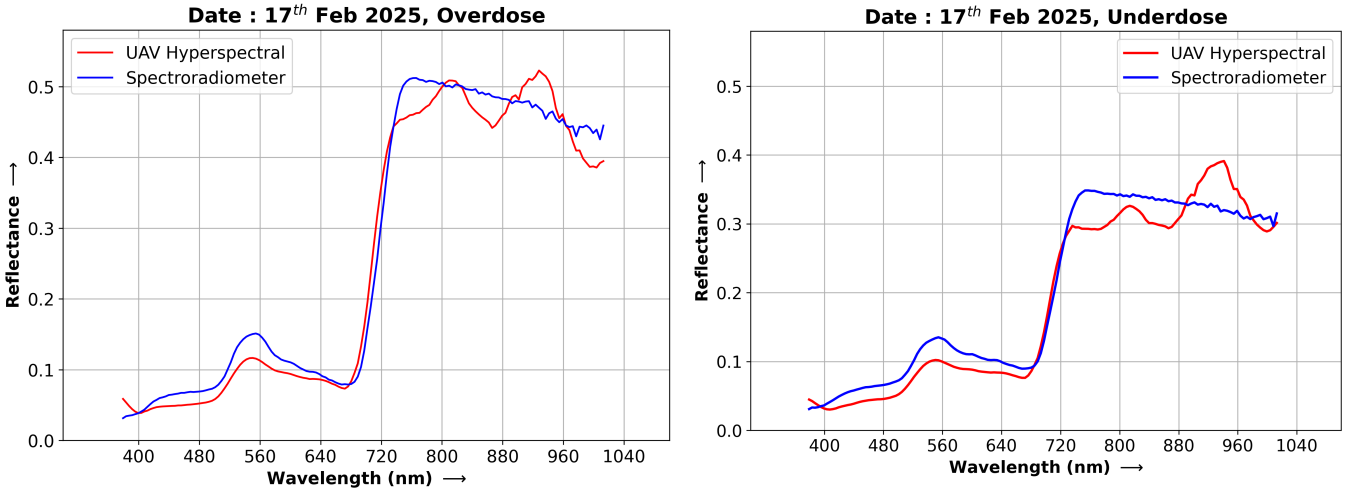


Figure 5.7: Normalized reflectance spectra obtained from UAV-based hyperspectral imagery for underdose, control, and overdose treatments averaged over subplots with the same nitrogen treatment. The shaded region represents the standard deviation among treatment replicates.

5.6 Comparison of hyperspectral sensor and spectroradiometer measurements

A comparison between UAV-based hyperspectral sensor output and handheld spectroradiometer measurements reveals a high degree of spectral agreement post-irradiance normalization. The spectral agreement was confirmed by very high Pearson correlation values. The results are shown in Figure 5.8.



(a) (b)

Figure 5.8: (**A**) Spectral comparison between UAV-based hyperspectral data and handheld spectroradiometer data post irradiance normalisation for the overdose nitrogen treatment, showing strong agreement in terms of Pearson correlation: r = 0.9913. (**B**) Spectral comparison for the underdose nitrogen treatment, also indicating high consistency between both sensors in terms of Pearson correlation: r = 0.9841.

Both sensors capture key vegetation reflectance features, such as the red-edge transition (700 nm) and near-infrared plateau, crucial for vegetation health assessment. The slight variations observed in the raw spectra are likely due to differences in sensor calibration, viewing geometry, and atmospheric conditions. Nevertheless, the overall spectral congruence validates the accuracy of UAV hyperspectral data in representing ground-truth reflectance (57). This alignment is critical for scaling plot-level spectral indices to field-wide assessments, enabling robust stress detection and vegetation monitoring at larger scales (58).

5.7 Temporal spectral variation and disease progression in soybean

To analyse the progression of disease in soybean, UAV-based hyperspectral data were acquired on three different dates: 2^{nd} Aug 2025 (healthy condition), 6^{th} Aug 2025 (slightly affected), and 12^{th} Aug 2025 (early disease symptoms visible). The UAV image of the experimental field is shown in Figure 5.9, followed by the spectral comparison across the three dates in Figure 5.10.

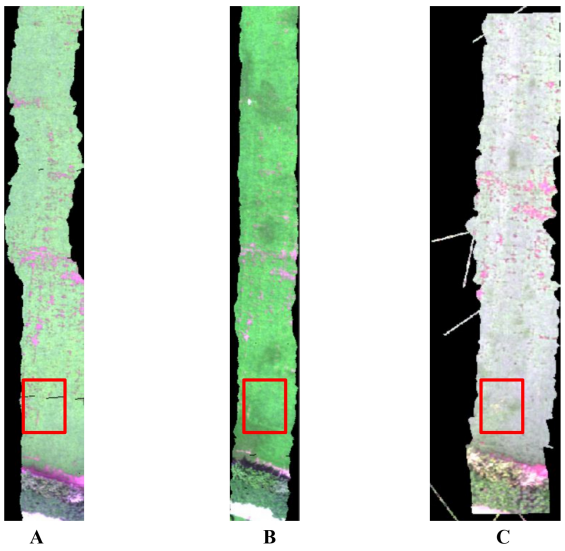


Figure 5.9: Hyperspectral image of the soybean experimental field showing spatial variability in crop condition across the study area. A) 2^{nd} Aug 2025, B) 6^{th} Aug 2025, C) 12^{th} Aug 2025

The temporal variation in spectral reflectance is presented in Fig. 5.10. On 2^{nd} Aug 2025, the crop was healthy, and the reflectance curve exhibits a typical vegetation signature, with low reflectance in the visible region and a steady increase in the near-infrared (NIR) region.

By 6^{th} Aug 2025, slight variations in reflectance are observed, particularly in the visible and red-edge regions, indicating the initial onset of stress, although no clear visual symptoms were evident in the field.

A more pronounced change is observed on 12^{th} Aug 2025, where the reflectance values are significantly higher, especially in the NIR region. This increase in reflectance is associated with changes in canopy structure and reduced chlorophyll absorption due to disease development. These spectral differences were also consistent with field observations, where early disease symptoms began to appear during this stage.

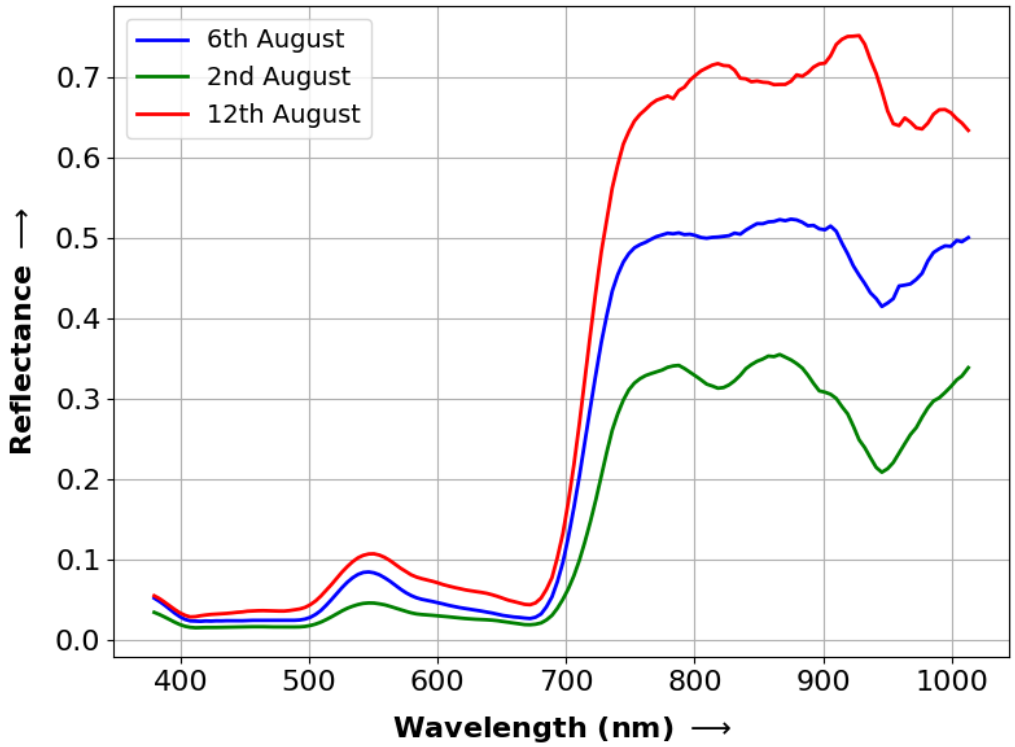


Figure 5.10: Temporal variation in hyperspectral reflectance of soybean canopy on 2^{nd} Aug 2025 (healthy), 6^{th} Aug 2025 (slightly affected), and 12^{th} Aug 2025 (early disease stage). A clear increase in reflectance, particularly in the NIR region, is observed as the disease progresses.

Overall, the temporal analysis demonstrates that hyperspectral data can capture subtle changes in plant condition before and during the early stages of disease development, making it an effective tool for early disease detection in soybean.

Chapter 6

CONCLUSION

This study demonstrated the potential of UAV-based hyperspectral imaging combined with ground-based spectroradiometer measurements for monitoring nitrogen stress in wheat and early disease detection in soybean. The temporal variation in the reflectance of the control, underdose, and overdose treatments is clearly visible and can be used for early-stage nitrogen detection. Several nitrogen-sensitive wavelengths were identified, including 642.4, 646.6, 650.8, 655.0, 659.2, 663.5, 667.7, 672.0, 676.2, 680.5, 684.7, 689.0, 693.2, 697.5, 701.7, and 706.0 nm, which showed greater discrimination among the nitrogen treatments.Time-series of various nitrogen-sensitive vegetation indices such as the NDVI, NDRE, ND_{705}, $CL_{red-edge}$, and DATT clearly differentiated between nitrogen treatments, with higher values consistently observed in nitrogen-overdose plots, reflecting improved canopy vigour and nitrogen content. The time-series for these indices also indicate variation for the different nitrogen treatments at early and later growth stages. The crop was sown on 3^{rd} Jan 2025, and differences among the nitrogen treatments became evident by 28^{th} Feb 2025. The variation among the under-dose, recommended-dose, and over-dose treatments was also statistically supported by ANOVA. These results indicate that hyperspectral data were sensitive to subtle changes in crop spectral response caused by different nitrogen levels. The findings are consistent with previous studies reporting the usefulness of hyperspectral and red-edge information for assessing nitrogen status in wheat. Compared with conventional vegetation indices, hyperspectral data provide information across a wider range of wavelengths, which can help capture subtle nitrogen-related changes. Therefore, UAV hyperspectral imagery can serve as a useful early-warning approach for identifying nitrogen stress before the symptoms become strongly visible. Overall, the integration of UAV hyperspectral technology with spectral analysis offers a scalable and non-destructive approach to improve nitrogen use efficiency, early-stage nitrogen detection, and crop productivity in wheat cultivation. A demonstration of the early detection of nitrogen stress in wheat showed that a high correlation between UAV-based hyperspectral data and handheld spectroradiometer data was obtained. The second study demonstrated the po-

tential of UAV-based hyperspectral imaging for early detection of soybean disease under real field conditions. By analysing temporal hyperspectral datasets acquired at three stages mainly healthy, slightly affected, and early symptomatic the study showed that spectral reflectance patterns change consistently with disease progression. Healthy plants exhibited a typical vegetation signature, while early-stage disease conditions showed noticeable variations, particularly in the visible, red-edge, and near-infrared regions. Unlike many previous studies that rely on controlled environments or detached leaf analysis, this work was conducted under actual field conditions, making the findings more practical and applicable to real-world agricultural scenarios. The use of UAV-mounted hyperspectral sensors also enables rapid, non-destructive, and large-scale monitoring, which is essential for precision agriculture.

Chapter 7

FUTURE WORK

This study primarily focused on nutrient stress associated with nitrogen in wheat. In the future, detailed investigations on phosphorus and potassium nutrient stress will be conducted to provide a more holistic understanding of plant responses under different nutrient stresses. Such studies may help identify distinct spectral and physiological changes linked to multiple macronutrient stresses. Furthermore, during the present study, yield data could not be collected as the experimental farm was damaged by Indian hare (*Lepus nigricollis*) at the maturity stage of the crop, resulting in complete loss of crop. Hence, analysis of the impact of nutrient stress on the final crop yield could not be carried out. In future studies, appropriate protective measures will be adopted to safeguard the crop during the critical maturity phase, enabling the collection of reliable yield data and strengthening the agronomic relevance of the findings. Additionally, the impact of nutrient stress on crop yield can be explored to establish stronger agronomic significance. Examining the relationship between nutrient deficiency, plant health indicators, and final yield will further support the practical applicability of this work in precision agriculture and crop management. In future, Machine learning and deep learning models can be used to automate disease detection instead of relying only on spectral comparison, making the approach more practical for larger areas. The study can also be carried out over multiple crop seasons and different environmental conditions to check how consistent these spectral patterns remain. Further, including other soybean diseases, both viral and fungal, will help in developing a more complete and reliable detection framework. The use of vegetation indices, especially those based on the red-edge region, can be explored in more detail to improve sensitivity to early stress. Combining hyperspectral data with other sensors such as thermal or multispectral cameras may also improve detection accuracy. Finally, moving towards a near real-time UAV-based system would make this approach more useful at the field level, allowing timely decisions and better crop management.

References

[1] R. Kundu, D. Dutta, M. K. Nanda, and A. Chakrabarty, "Near real time monitoring of potato late blight disease severity using field based hyperspectral observation," *Smart Agricultural Technology*, vol. 1, p. 100019, 2021.

[2] P. C. Doraiswamy, S. Moulin, P. W. Cook, and A. Stern, "Crop yield assessment from remote sensing," *Photogrammetric engineering & remote sensing*, vol. 69, no. 6, pp. 665–674, 2003.

[3] Y. Peng, T. Zhu, Y. Li, C. Dai, S. Fang, Y. Gong, X. Wu, R. Zhu, and K. Liu, "Remote prediction of yield based on lai estimation in oilseed rape under different planting methods and nitrogen fertilizer applications," *Agricultural and forest meteorology*, vol. 271, pp. 116–125, 2019.

[4] S. Francesconi, A. Harfouche, M. Maesano, and G. M. Balestra, "Uav-based thermal, rgb imaging and gene expression analysis allowed detection of fusarium head blight and gave new insights into the physiological responses to the disease in durum wheat," *Frontiers in plant science*, vol. 12, p. 628575, 2021.

[5] B. Shiferaw, M. Smale, H.-J. Braun, E. Duveiller, M. Reynolds, and G. Muricho, "Crops that feed the world 10. past successes and future challenges to the role played by wheat in global food security," *Food security*, vol. 5, no. 3, pp. 291–317, 2013.

[6] Food and Agriculture Organization of the United Nations (FAO), "Fao statistics." https://www.fao.org/statistics/en/, 2021. [Accessed 28 July 2022].

[7] Y. Zhu, Y. Tian, X. Yao, X. Liu, and W. Cao, "Analysis of common canopy reflectance spectra for indicating leaf nitrogen concentrations in wheat and rice," *Plant Production Science*, vol. 10, no. 4, pp. 400–411, 2007.

[8] L. Xue, H. Zhang, L. Zhang, Y. Zhu, W. Cao, X. Yao, and Y. Tian, "Predicting leaf nitrogen content in wheat with canopy hyperspectral reflectance," *Field Crops Research*, vol. 233, pp. 11–19, 2019.

[9] R. F. Muñoz-Huerta, R. G. Guevara-Gonzalez, L. M. Contreras-Medina, I. Torres-Pacheco, J. Prado-Olivarez, and R. V. Ocampo-Velazquez, "A review of methods for sensing the nitrogen status in plants: Advantages, disadvantages and recent advances," *Sensors*, vol. 13, no. 8, pp. 10823–10843, 2013.

[10] A. G. Good and P. H. Beatty, "Fertilizing nature: A tragedy of excess in the commons," *PLoS Biology*, vol. 9, no. 8, p. e1001124, 2011.

[11] J. P. Baresel, G. Zimmermann, and H. J. Reents, "Effects of genotype and environment on n uptake and n partition in organically grown winter wheat (triticum aestivum l.) in germany," *Euphytica*, vol. 163, no. 3, pp. 347–354, 2008.

[12] J. Sun, H. Mooney, W. Wu, H. Tang, Y. Tong, Z. Xu, B. Huang, Y. Cheng, X. Yang, and D. Wei, "Importing food damages domestic environment: Evidence from global soybean trade," *Proceedings of the National Academy of Sciences*, vol. 115, no. 21, pp. 5415–5419, 2018.

[13] G. L. Hartman, E. D. West, and T. K. Herman, "Crops that feed the world 2. soybean—worldwide production, use, and constraints caused by pathogens and pests," *Food Security*, vol. 3, no. 1, pp. 5–17, 2011.

[14] R. Tayade, A. Ghimire, W. Khan, L. Lay, J. Q. Attipoe, and Y. Kim, "Silicon as a smart fertilizer for sustainability and crop improvement," *Biomolecules*, vol. 12, no. 8, p. 1027, 2022.

[15] M. G. Roth, R. W. Webster, D. S. Mueller, M. I. Chilvers, T. R. Faske, F. M. Mathew, C. A. Bradley, J. P. Damicone, M. Kabbage, and D. L. Smith, "Integrated management of important soybean pathogens of the united states in changing climate," *Journal of Integrated Pest Management*, vol. 11, no. 1, p. 17, 2020.

[16] N. J. Ngwangum, R. Tayade, L. Liny, J.-B. Yoon, Y.-S. Chung, and Y. Kim, "Utilization of imaging data from different sources for bacterial and fungal diseases detection in major crops in the digital era: A review," *Journal of Agriculture and Life and Environment Sciences*, pp. 97–117, 2022.

[17] N. Sandra, A. Tripathi, S. Lal, B. Mandal, and R. K. Jain, "Molecular and biological characterization of soybean yellow mottle mosaic virus severe strain infecting soybean in india," *3 Biotech*, vol. 11, pp. 1–12, 2021.

[18] P. K. Amrate, M. K. Shrivastava, and D. K. Pancheshwar, "Yield reduction and efficacy of antiviral product against yellow mosaic virus disease in soybean," *Journal of Crop and Weed*, vol. 8, pp. 27–34, 2020.

[19] A. D. Ziems, L. J. Giesler, G. L. Graef, M. G. Redinbaugh, J. L. Vacha, S. Berry, L. V. Madden, and A. E. Dorrance, "Response of soybean cultivars to bean pod mottle virus infection," *Plant Disease*, vol. 91, no. 6, pp. 719–726, 2007.

[20] S. Li, J. S. Moon, S. H. Lee, and L. L. Domier, "First report of soybean yellow mottle mosaic virus in soybean in north america," *Plant Disease*, vol. 93, no. 11, pp. 1214–1214, 2009.

[21] M. Nam, S.-M. Kim, L. L. Domier, S. Koh, J.-K. Moon, H.-S. Choi, H.-G. Kim, J.-S. Moon, and S.-H. Lee, "Nucleotide sequence and genomic organization of a newly identified member of the genus carmovirus, soybean yellow mottle mosaic virus, from soybean," *Archives of Virology*, vol. 154, no. 10, pp. 1679–1684, 2009.

[22] Y. Yoon, S. Lim, Y.-W. Jang, B.-S. Kim, D.-H. Bae, R. Maharjan, H. Yi, S. Bae, Y.-H. Lee, and B.-C. Lee, "First report of soybean mosaic virus and soybean yellow mottle mosaic virus in *Vigna angularis*," *Plant Disease*, vol. 102, no. 4, pp. 689–689, 2018.

[23] M. M. Kabir, A. Q. Ohi, and M. F. Mridha, "A multi-plant disease diagnosis method using convolutional neural network," in *Computer Vision and Machine Learning in Agriculture*, pp. 99–111, Springer, 2021.

[24] S. D. Khirade and A. B. Patil, "Plant disease detection using image processing," in *Proceedings of the 2015 International Conference on Computing Communication Control and Automation*, pp. 768–771, 2015.

[25] R. R. Navalgund, V. Jayaraman, and P. Roy, "Remote sensing applications: An overview," *current science*, pp. 1747–1766, 2007.

[26] E. Omia, H. Bae, E. Park, M. S. Kim, I. Baek, I. Kabenge, and B.-K. Cho, "Remote sensing in field crop monitoring: A comprehensive review of sensor systems, data analyses and recent advances," *Remote Sensing*, vol. 15, no. 2, p. 354, 2023.

[27] P. S. Thenkabail, J. G. Lyon, and A. Huete, *Hyperspectral Remote Sensing of Vegetation*. Boca Raton, FL: CRC Press, 2013.

[28] M. L. Gnyp, Y. Miao, F. Yuan, S. L. Ustin, K. Yu, Y. Yao, and G. Bareth, "Hyperspectral canopy sensing of crop nitrogen status: Prospects and limitations," *Advances in Agronomy*, vol. 121, pp. 149–186, 2014.

[29] R. N. Sahoo, R. G. Rejith, S. Gakhar, R. Ranjan, M. C. Meena, A. Dey, J. Mukherjee, R. Dhakar, A. Meena, A. Daas, S. Babu, P. K. Upadhyay, K. Sekhawat, S. Kumar, M. Kumar, V. Chinnusamy, and M. Khanna, "Drone remote sensing of wheat n using hyper-

spectral sensor and machine learning," *Precision Agriculture*, vol. 25, no. 2, pp. 704–728, 2023.

[30] Y.-Z. Feng and D.-W. Sun, "Application of hyperspectral imaging in food safety inspection and control: A review," *Critical Reviews in Food Science and Nutrition*, vol. 52, no. 11, pp. 1039–1058, 2012.

[31] G. Mahajan, R. Pandey, R. Sahoo, V. Gupta, S. Datta, and D. Kumar, "Monitoring nitrogen, phosphorus and sulphur in hybrid rice (oryza sativa l.) using hyperspectral remote sensing," *Precision agriculture*, vol. 18, pp. 736–761, 2017.

[32] P. Benincasa, S. Antognelli, L. Brunetti, C. A. Fabbri, A. Natale, V. Sartoretti, G. Modeo, M. Guiducci, F. Tei, and M. Vizzari, "Reliability of ndvi derived by high resolution satellite and uav compared to in-field methods for the evaluation of early crop n status and grain yield in wheat," *Experimental Agriculture*, vol. 54, no. 4, pp. 604–622, 2018.

[33] F. Yu, J. Bai, Z. Jin, H. Zhang, J. Yang, and T. Xu, "Estimating the rice nitrogen nutrition index based on hyperspectral transform technology," *Frontiers in plant science*, vol. 14, p. 1118098, 2023.

[34] H. Tao, H. Feng, L. Xu, M. Miao, G. Yang, X. Yang, and L. Fan, "Estimation of the yield and plant height of winter wheat using uav-based hyperspectral images," *Sensors*, vol. 20, no. 4, p. 1231, 2020.

[35] A. Moghimi, *Integrating Hyperspectral Imaging and Artificial Intelligence to Develop Automated Frameworks for High-throughput Phenotyping in Wheat*. PhD thesis, University of Minnesota, 2019.

[36] A. K. Sharma, S. K. Sidhu, A. Singh, L. Zotarelli, and L. K. Sharma, "Optimizing uav hyperspectral imaging for predictive analysis of nutrient concentrations, biomass growth, and yield prediction of potatoes," *American Journal of Potato Research*, vol. 101, no. 5, pp. 394–413, 2024.

[37] N. Mantri, V. Patade, S. Penna, R. Ford, and E. Pang, "Abiotic stress responses in plants: present and future," *Abiotic stress responses in plants: metabolism, productivity and sustainability*, pp. 1–19, 2012.

[38] X. Zhou, W. Huang, W. Kong, H. Ye, J. Luo, and P. Chen, "Remote estimation of canopy nitrogen content in winter wheat using airborne hyperspectral reflectance measurements," *Advances in Space Research*, vol. 58, no. 9, pp. 1627–1637, 2016.

[39] H. Zhu, H. Liu, Y. Xu, and G. Yang, "Uav-based hyperspectral analysis and spectral indices constructing for quantitatively monitoring leaf nitrogen content of winter wheat," *Applied Optics*, vol. 57, no. 27, pp. 7722–7732, 2018.

[40] H. Liu, H. Zhu, and P. Wang, "Quantitative modelling for leaf nitrogen content of winter wheat using uav-based hyperspectral data," *International Journal of Remote Sensing*, vol. 38, no. 8–10, pp. 2117–2134, 2017.

[41] J. Zhang, T. Cheng, L. Shi, W. Wang, Z. Niu, W. Guo, and X. Ma, "Combining spectral and texture features of uav hyperspectral images for leaf nitrogen content monitoring in winter wheat," *International Journal of Remote Sensing*, vol. 43, no. 7, pp. 2335–2356, 2022.

[42] B.-B. Guo, Y.-J. Zhu, W. Feng, L. He, Y.-P. Wu, Y. Zhou, X.-X. Ren, and Y. Ma, "Remotely estimating aerial n uptake in winter wheat using red-edge area index from multi-angular hyperspectral data," *Frontiers in Plant Science*, vol. 9, p. 675, 2018.

[43] A. Guo, W. Huang, Y. Dong, H. Ye, H. Ma, B. Liu, M. Wu, and Y. Geng, "Integration of canopy pigments and spectral indices from uav hyperspectral imagery for early detection of wheat stripe rust," *Computers and Electronics in Agriculture*, vol. 216, p. 108500, 2024.

[44] D. Zhang, D. Wang, C. Gu, N. Jin, H. Zhao, G. Chen, D. Liang, and D. Liang, "Deep learning-based speed-up and pixel-level quantitative regression for wheat stripe rust monitoring using uav-based hyperspectral images," *Remote Sensing*, vol. 15, no. 9, p. 2320, 2023.

[45] J. Abdulridha, Y. Ampatzidis, J. Qureshi, and P. Roberts, "Laboratory and uav-based identification and classification of tomato diseases using hyperspectral imaging and machine learning," *Remote Sensing*, vol. 12, no. 6, p. 952, 2020.

[46] S. Ghosal, D. Blystone, A. K. Singh, B. Ganapathysubramanian, A. Singh, and S. Sarkar, "An explainable deep machine learning framework for plant stress phenotyping," *Proceedings of the National Academy of Sciences*, vol. 115, no. 18, pp. 4613–4618, 2018. Reference [7]: Greenhouse/benchtop soybean disease detection.

[47] K. Nagasubramanian, S. Jones, A. K. Singh, A. Singh, B. Ganapathysubramanian, and S. Sarkar, "Hyperspectral phenotype classification using deep convolutional neural network," *Plant Methods*, vol. 15, pp. 1–14, 2019. Reference [8]: Controlled illumination soybean disease detection.

[48] S. Jain, U. Khati, V. Kumar, and R. Verma, "Detection of soybean pod formation stage using sentinel-1 sar data," *IEEE Journal of Selected Topics in Applied Earth Observations and Remote Sensing*, 2024.

[49] A. F. Almeida-Ñauñay, A. M. Tarquis, J. Lopez-Herrera, E. Perez-Martin, J. L. Pancorbo, M. D. Raya-Sereno, and M. Quemada, "Optimization of soil background removal to improve the prediction of wheat traits with uav imagery," *Computers and Electronics in Agriculture*, vol. 205, p. 107559, 2023.

[50] Q. Li, M. Gao, and Z.-L. Li, "Ground hyper-spectral remote-sensing monitoring of wheat water stress during different growing stages," *Agronomy*, vol. 12, no. 10, p. 2267, 2022.

[51] X. Cao, Q. Chen, B. Liu, S. Cheng, Y. Miao, G. Feng, S. Yue, F. Li, C. Yang, and J. A. Anderson, "Estimation of winter wheat plant nitrogen concentration from uav hyperspectral remote sensing combined with machine learning methods," *Remote Sensing*, vol. 15, no. 11, p. 2831, 2023.

[52] L. Zhang, Y. Shen, X. Liu, Y. Zhang, J. Wang, and H. Shi, "Hyperspectral estimation of nitrogen content in wheat based on fractional difference and continuous wavelet transform," *Agriculture*, vol. 13, no. 5, p. 1017, 2022.

[53] G. Rondeaux, M. Steven, and F. Baret, "Optimized soil-adjusted vegetation index (osavi)," *Remote Sensing of Environment*, vol. 55, no. 1, pp. 19–34, 1996.

[54] C. Buschmann, S. Lenk, and H. K. Lichtenthaler, "Reflectance spectra and images of green leaves with different tissue structure and chlorophyll content," *Israel Journal of Plant Sciences*, vol. 60, no. 1-2, pp. 49–64, 2012.

[55] C. Tan, Y. Du, J. Zhou, D. Wang, M. Luo, Y. Zhang, and W. Guo, "Analysis of different hyperspectral variables for diagnosing leaf nitrogen accumulation in wheat," *Frontiers in Plant Science*, vol. 9, p. 674, 2018.

[56] J. G. Clevers and L. Kooistra, "Using hyperspectral remote sensing data for retrieving canopy chlorophyll and nitrogen content," *IEEE Journal of selected topics in applied earth observations and remote sensing*, vol. 5, no. 2, pp. 574–583, 2011.

[57] P. S. Thenkabail, I. Mariotto, M. K. Gumma, E. M. Middleton, D. R. Landis, and K. F. Huemmrich, "Selection of hyperspectral narrowbands (hnbs) and composition of hyperspectral twoband vegetation indices (hvis) for biophysical characterization and discrimination of crop types using field reflectance and hyperion/eo-1 data," *IEEE Journal of Selected Topics in Applied Earth Observations and Remote Sensing*, vol. 6, no. 2, pp. 427–439, 2013.

[58] M. Awais, W. Li, M. Cheema, Q. Zaman, A. Shaheen, B. Aslam, W. Zhu, M. Ajmal, M. Faheem, S. Hussain, *et al.*, "Uav-based remote sensing in plant stress imagine using high-resolution thermal sensor for digital agriculture practices: A meta-review," *International Journal of Environmental Science and Technology*, vol. 20, no. 1, pp. 1135–1152, 2023.